Natural Resources Canada | Ressources naturelles Canada

GEOLOGICAL SURVEY OF CANADA
OPEN FILE 8904

Borehole electrical resistivity, Vars–Winchester esker aquifer, Ontario

G.A. Oldenborger

2022

Canada

ISSN 2816-7155
ISBN 978-0-660-44273-0
Catalogue No. M183-2/8904E-PDF

GEOLOGICAL SURVEY OF CANADA
OPEN FILE 8904

Borehole electrical resistivity, Vars–Winchester esker aquifer, Ontario

G.A. Oldenborger

2022

Permanent link: https://doi.org/10.4095/330299

This publication is available for free download through GEOSCAN (https://geoscan.nrcan.gc.ca/).

Recommended citation
Oldenborger, G.A., 2022. Borehole electrical resistivity, Vars–Winchester esker aquifer, Ontario; Geological Survey of Canada, Open File 8904, 44 p. https://doi.org/10.4095/330299

Publications in this series have not been edited; they are released as submitted by the author.

SUMMARY

Electrical resistivity and induced polarization surveys were conducted for a portion of the Vars-Winchester esker aquifer system near Embrun, Ontario. Resistivity data were acquired within boreholes as 1D logs, along the surface as 2D profiles, and from surface-to-borehole as 3D volumes. Borehole logs and pseudo-logs of electrical resistivity and chargeability from these surveys are compared to borehole geophysical logs, lithological logs, and hydraulic conductivity measurements collected at the study site. The resistivity records are in nominal agreement with electromagnetic induction logs of apparent resistivity, but there are significant differences attributed to scale and an anisotropy factor of approximately 2. Estimates of petrophysical model parameters and surface conductivity derived using the borehole fluid conductivity logs are not reliable. However, the borehole induction logs and pseudo-logs recovered from 1D, 2D, and 3D surveys all exhibit some separability of resistivity in terms of lithology that can be used for geological classification, and some correlation of resistivity with hydraulic conductivity that can be used for prediction away from the boreholes. Fidelity may be limited to the approximate distinction of aquifer versus aquiclude, particularly for the lowest-resolution 2D surface surveys.

TABLE OF CONTENTS

INTRODUCTION

Electrical resistivity experiments can be applied to investigate aquifer structure and aquifer properties due to the dependence of electrical properties on sediment type, texture, porosity, and pore water (Slater, 2007). Measurements of electrical resistivity (the inverse of electrical conductivity) can be used for qualitative interpretation of aquifer morphology or internal structure, and have been used to map and model Quaternary aquifer systems (Steuer et al., 2009; Siemon et al., 2009; Oldenborger et al., 2013; Sapia et al., 2015). Given additional information on hydrogeologic parameters, electrical resistivity measurements can be used as part of a more quantitative hydrogeophysical prediction of aquifer properties (Foged et al., 2013; Weller et al., 2015; Revil et al., 2017; Glaser, 2021) or to estimate salinity, porosity, or other parameters via petrophysical transforms (Hyde and Hunter, 1998; Oldenborger et al., 2007; Glover, 2016). However, calibrations or petrophysical modelling performed using sample or borehole measurements (point-based or 1D) may suffer from inconsistencies when used for extrapolation (to 2D or 3D) due to differences in geophysical survey types, geometries, and scales.

Electrical resistivity and induced polarization surveys were conducted for a portion of the Vars-Winchester esker aquifer system near Embrun, Ontario as part of a larger initiative for hydrogeological and geophysical investigation of the aquifer and aquiclude (Paradis et al., 2020). Resistivity data were acquired within boreholes as 1D logs, along the surface as 2D profiles, and from surface-to-borehole as 3D volumes (Oldenborger, 2021). Borehole logs and pseudo-logs of electrical resistivity are extracted from the results of these surveys for comparison to geophysical borehole logs collected at the study area including electromagnetic induction, fluid conductivity, and porosity (Crow et al., 2020). This comparison allows for validation and qualification of electrical resistivity survey results, as well as testing of petrophysical models. Electrical resistivity is also compared to borehole lithological logs and packer-based slug test hydraulic conductivity measurements (Crow et al., 2022) to examine the predictive capacity of electrical resistivity and normalized chargeability.

STUDY AREA

Electrical resistivity surveys were conducted over a 2 km × 4 km area of South Nation River watershed near Embrun, Ontario (Figure 1). The study area represents a small portion of the Vars-Winchester esker aquifer system exploited by the communities of Vars and Limoges for municipal drinking water, along with many domestic and agricultural users. The aquifer system consists of an esker approximately 50 km in length comprised of a largely carbonate gravel core

with coarse sand matrix covered by sand extending a few hundred meters in width (Cummings and Russel, 2007; Pugin et al., 2009; Sauriol, 2016). The esker is buried along most of its length by fine marine muds deposited during inundation by the post-glacial Champlain Sea. The esker erosively overlies a thin till sheet (not everywhere present) and Paleozoic carbonate or shale bedrock with a fractured upper surface (Cummings et al., 2011).

The Champlain Sea sediments can have high salinity (Torrance, 1983; Crow et al., 2017) and may be highly conductive, despite low connected porosity. A large component of the conductivity may result from grain surface conduction (Hyde and Hunter, 1998) that may be manifest as an induced polarization response (e.g., Weller et al., 2013). In contrast, the pore waters within the esker sands and gravels are relatively fresh resulting in lower electrical conductivity, despite a higher connected porosity. Geophysical logs collected within the Vars-Winchester esker aquifer system confirm these general characteristics while providing evidence of additional internal complexity within the sedimentary units (Crow et al., 2020).

METHODS

Electrical resistivity surveys

Direct-current (DC) electrical resistivity and induced polarization surveys are a well-established geophysical method that involve galvanic injection of a known electrical current into the subsurface, and measurement of the resulting potential distribution via surface and/or borehole electrodes. Electrical resistivity and time-domain induced polarization data were collected in October 2018 for the Vars-Winchester aquifer using 1D borehole acquisition, 2D surface acquisition, and 3D surface-to-borehole acquisition. Full details of acquisition, processing, inversion, and results are given by Oldenborger (2021).

Borehole electrical resistivity data were collected from below the water table to depths of 36–38 m with 1 m electrode spacing in four fully-screened boreholes (142 mm diameter with 115 mm PVC casing), three of which represent a cross section perpendicular to the esker (Figure 1). Measurements of transfer resistance were filtered and converted directly to borehole logs of 1D apparent resistivity ρ_{1D} using a whole-space geometric factor with image electrodes. Decay voltages were integrated, filtered and normalized to yield borehole logs of 1D integral chargeability M and resistivity-normalized integral chargeability M_n with the latter being approximately proportional to both the out-of-phase electrical conductivity and the in-phase surface conductivity (Weller et al., 2013; Revil et al., 2017). The quadrupoles were 3 m in length

with a median signal strength radius of approximately 40 cm (e.g., Edwards, 1977). The logs are reported at the mid-points of the 4-electrode measurements. Although the 1D apparent resistivity logs have error estimates associated with data acquisition, they are small and more representative of instrument precision rather than true uncertainty.

Surface electrical resistivity data were collected along roadsides both cross- and along-strike to the esker with 5 m electrode spacing (Figure 1). Surface measurements of transfer resistance and integral chargeability were filtered and inverted using 2D least-squares inversion. The inverse model cell sizes were set at 2.5 m in the horizontal direction, and 1.25 m in the vertical direction for the surface layer with electrodes at cell edges. Model cell thickness was increased with depth to approximately 3 m at 30 m depth. All measurements and the recovered 2D electrical resistivity model were converted to elevation to account for borehole-road offsets and variation in surface elevation between boreholes. Borehole pseudo-logs of 2D resistivity ρ_{2D} were extracted from the recovered resistivity models for the cell centre elevations at the borehole locations. Although integral chargeability was measurable for the surface surveys, the 2D recovered chargeability models are mostly noisy or homogeneous and are not considered herein.

Surface-to-borehole resistivity data were collected using a combination of borehole electrodes below the water table with 1 m electrode spacing, and electrodes on the ground surface extending in two directions away from the borehole also with 1 m electrode spacing. The surface-to-borehole measurements were filtered and inverted using 3D least-squares inversion with uniform cell sizes of 1 m in all directions except at the boreholes, which were explicitly meshed using cell sizes of 10 cm in the horizontal directions with a geometric transition to 1 m. Despite smoothing inherent to the inversion, the recovered 3D electrical resistivity models exhibit some vertical oscillation typical of near-electrode inversion artefacts. To suppress these artefacts, pseudo-logs of 3D resistivity ρ_{3D} were extracted from the recovered resistivity models at the cell centre elevations for the borehole locations using a Gaussian-weighted spherical arithmetic average filter with a standard deviation of 50 cm (where arithmetic averaging implies isotropic series current flow). To remove the influence of the low-resistivity borehole water column, the filter excludes a cylindrical core with a radius of 15 cm. The filter has a peak response radius of 17 cm and an integrated half-response radius (50% quartile) of approximately 50 cm in the horizontal direction with 95% of the response coming from a radius of approximately 100 cm. The vertical extent at half-maximum is 120 cm (approximately 2.4 standard deviations). After filtering, there is still some vertical oscillation apparent in the 3D pseudo-logs that may be attributable to electrode effects, but more aggressive filtering might suppress actual geological variability. As with the surface surveys, the measured 3D integral chargeability was small for the surface-to-

borehole surveys and the data misfits associated with the inversions were high. Nevertheless, recovered 3D intrinsic chargeability m and the normalized 3D intrinsic chargeability m_n exhibit reasonable structure and were extracted as pseudo-logs from the recovered models in the same fashion as for resistivity.

Borehole Logs

The borehole data to which the electrical resistivity results are compared comprise geophysical logs of apparent resistivity, fluid resistivity, and porosity, along with packer-based hydraulic conductivity and lithological drill logs as described in more detail by Crow et al. (2020), Paradis et al. (2020), and Crow et al. (2022). The geophysical borehole logs have sample intervals ranging from 1–50 cm, but measurements are typically representative of larger support volumes.

Logs of apparent resistivity ρ_a are the inverse of apparent conductivity measurements made at 2 cm intervals using the Geonics EM39 electromagnetic induction tool operating at 39.2 kHz (McNeil, 1986). The EM39 has a response function characterized by a peak response radius of 28 cm, an integrated half-response radius of 58 cm, and a vertical extent at half-maximum of 65 cm. Logs of fluid resistivity ρ_f are records of galvanic electrical measurements made using a seven electrode mirrored Wenner array and converted to resistivity using a geometric factor. The electrode array has a dimension of approximately 5 cm and is contained within a protective nose cone, such that fluid resistivity measurements can be considered to be point-based and entirely in-hole. The porosity logs are records of clay-bound n_c, capillary-bound n_p, mobile n_m, and total porosity n obtained from processing of nuclear magnetic resonance (NMR) data measured using a Vista Clara Javelin JP238. The response function for the Javelin tool is specified as a cylindrical shell of 50 cm extent in the vertical direction with a diameter of 23–30 cm. Practical testing suggests a Gaussian-type response function with an integrated half-response at approximately 11 cm radius (H. Crow, personal communication). The hydraulic conductivity logs result from packer-isolated slug tests over 1 m intervals using approximately 4 m of displacement to stress a large volume around the borehole. The slug tests were inverted for horizontal hydraulic conductivity K_h (Crow et al., 2022). The lithological logs are based on observational analysis of cuttings collected during drilling and can have as much as 2 m vertical error (the length of the drill rod). Simplified sediment type was extracted from the drill logs: soil, unsaturated clay silt, clay silt, sand, sand and gravel, and shale. The borehole stratigraphy has been revised based on the suite of geophysical logs (Crow et al., 2020). However, the original observations from the drill logs are used herein to avoid the introduction of bias or circular dependency in calibration or labelling of other geophysical data.

Log Comparisons

To facilitate direct point-based comparison of the different records of electrical resistivity and the supporting data, all of the logs and pseudo-logs described above were interpolated via piece-wise cubic interpolation to 1 m intervals at the electrode elevations of the 3D surface-to-borehole surveys (equivalent to elevations of the ρ_{3D} pseudo-logs). Prior to interpolation, some records were filtered with a Gaussian low-pass filter to improve the frequency response of the interpolated logs (simple boxcar moving averages are not zero-phase and may induce significant feature migration). It can be shown that low-pass filtering of a nearly-continuous record with an already finite support volume results in double-filtering and a loss of fidelity, and should be avoided unless the down-sampled target resolution is much larger than the original support volume of the record.

The vertical target resolution was approximated as the support volume of the 3D pseudo-logs, but this is difficult to quantify exactly. It is some combination of the variable point-spread function of the 3D inversion (e.g., Oldenborger and Routh, 2009) and the cored spherical filter used to extract the pseudo-logs. The extraction filter was assumed to extend beyond the point-spread function, such that the width at half-maximum (approximately 120 cm) was used as the nominal target resolution, and the low-pass filter was prescribed the equivalent standard deviation of 50 cm. The low-pass filter was applied only to the logs with a vertical response function extent less than one-half that of the target vertical resolution, or 60 cm (ρ_f, n). The low-pass filter is akin to a weighted vertical arithmetic average that does not account for anisotropy or parallel current flow. The remaining logs (ρ_a, ρ_{1D}, ρ_{2D}, K) were interpolated without a low-pass filter (ρ_{3D} required no interpolation). Most of the logs are sufficiently smooth that the filtering procedure has only a small effect, suggesting that the property exhibits little variability (ρ_f) or that the true resolution of the record is larger than the nominal support volume (ρ_a, K, n).

Petrophysical Models

Petrophysical models are often cast in terms of conductivity (the inverse of resistivity) to allow for the summation of terms associated with parallel current flow. The total ohmic conductivity measured in the field can be expressed as the sum of the surface conductivity and the electrolytic conductivity as

$$\sigma_T = \sigma_s + \sigma_e = \sigma_s + \frac{\sigma_f}{F} \quad (1)$$

where σ_f is the fluid conductivity, F is the electrolytic formation factor, and the out-of-phase (complex) conductivity has been neglected (e.g., Slater, 2007). The formation factor is further expressed using a modified Archie's law

$$F = \sigma_f / \sigma_e = a n^{-c} \quad (2)$$

where $\sigma_e = \sigma_T - \sigma_s$, c is the porosity exponent, and a is a fitting factor that accommodates for experimental error as described by Glover (2015; 2016). For Archie-type rocks and unconsolidated sediments, the formation factor is approximately constant for a particular lithology. As such, given measurements of fluid conductivity, a linear fit can be applied to the measured σ_T versus σ_f for which the slope provides an ensemble estimate of F^{-1} and the intercept provides a constant σ_s. Given σ_s and independent measurements of n, sample-based estimates and averages of F and c can be calculated from equation (2) for $a = 1$. However, Glover (2016) argues that a more accurate ensemble estimate of the porosity exponent can be obtained via a linear fit to the equation

$$\log(F) = \log(a) - c \log(n) \quad (3)$$

where F is the sample-based formation factor, and the nearness of a to unity is a measure of data quality.

In practice, application of equations (1) through (3) requires measurements of fluid conductivity that are representative of the in-situ conditions as opposed to conditions in the borehole water column, and porosity measurements that are representative of the porosity available for electrolytic conduction. Furthermore, estimating an ensemble formation factor from equation (1) requires a spatially invariant formation factor to the extent that a linear fit is warranted. Similarly, estimating surface conductivity from equation (1) requires a constant surface conductivity to the degree that some non-zero intercept is clear (even if a linear relationship is not evident) and representative over the entire range of fluid conductivity. In the event that one of these conditions is not met, the effect can be difficult to isolate. For example, an increase in surface conductivity with fluid conductivity will increase the slope of equation (1) resulting in overestimation of the formation factor; it may also reduce the linear intercept resulting in underestimation of surface conductivity (even to negative values).

When drilling logs or similar data are available, petrophysical analysis can be performed separately for each lithology. However, it may still be the case that any of the surface conductivity, porosity, or porosity exponent exhibits variability sufficient to preclude linear fitting of equations (1) to (3). In such a case, one option is to perform non-linear fitting of equations (1) and (2) for constant σ_s and c with $a = 1$. Alternatively, for low fluid conductivity, surface conductivity can be estimated based on the minimum total conductivity. For high fluid

conductivity, a constant formation factor can be estimated with the assumption that surface conductivity is negligible. Using this technique, Weller et al., (2013) calculate variable surface conductivity by differencing equation (1) and demonstrate a linear proportionality to normalized chargeability of $\sigma_s = 5\, m_n$ such that surface conductivity can also be estimated from independent measurements of chargeability.

RESULTS

The resistivity logs and pseudo-logs are illustrated in Figures 2–5 along with hydraulic conductivity, major lithostratigraphic contacts, and the water level at the time of the electrical resistivity surveys (which may differ from that at the time of drilling and borehole geophysical logging). The resistivity logs, pseudo-logs, and geophysical logs resampled to common elevations and used for point-based comparisons are presented in Appendix A. Approximately 25–30 m elevation corresponds to the maximum depth of investigation for the surface-to-borehole surveys, and approximately 30–40 m elevation corresponds to the maximum depth of investigation for the surface surveys (Oldenborger, 2021).

In visually comparing the logs and pseudo-logs, it is apparent that there is general agreement between the resistivity records in terms of resistive and conductive regions, but there is significant disagreement in the actual values of resistivity, with perhaps the most pronounced differences observed for BH4 (Figure 5). Furthermore, the difference in resistivity seems to be greater within the sands and gravels at higher resistivity, although the relative difference may be the same (see below). The EM39 apparent resistivity ρ_a and the 3D resistivity ρ_{3D} appear most similar, and the 2D resistivity ρ_{2D} appears most dissimilar. The extremely smooth nature of the 2D resistivity pseudo-logs is a product of the lower resolution surface-only data set and its inversion on a relatively coarse model mesh, especially at depth.

The point-based comparisons between the resistivity records are shown in Figure 6a for all boreholes and lithologies using ρ_a as a reference. For all but a handful of samples, the galvanic resistivities are consistently greater than the EM39 apparent resistivity. Linear correlation is generally high and the slopes of the linear fits range from approximately 2.0 for ρ_{3D} versus ρ_a, to 2.6 for ρ_{1D} versus ρ_a, and 4.1 for ρ_{2D} versus ρ_a. Although the slope is closest to unity for ρ_{3D}, the correlation coefficient his highest between ρ_{1D} and ρ_a (although the correlation between ρ_{3D} and ρ_a increases significantly to 0.87 with the removal of a single conspicuous outlier at $\rho_{3D} > 350$ Ωm).

There is similar visual agreement between the logs of 1D normalized integral chargeability M_n and the pseudo-log of 3D normalized intrinsic chargeability m_n (Figures 2–5). Both records exhibit low chargeability overall, but with some increased chargeability for clay silt and for sand and gravel near the shale contact. However, the point-based comparison between the normalized chargeability records reveals clustering at low chargeability, a slope significantly less than unity, and a large degree of scatter (Figure 6b). Nevertheless, the strength of the linear correlation is statistically significant, suggesting some degree of similar information content in both records.

Lithology

Visual inspection of the different resistivity records suggests a general lithological control on resistivity, with the sand and gravel being the most resistive, and the clay silt being the least resistive (Figures 2–5). There are some increases in ρ_{1D} and ρ_{3D} observed at the water table (Figures 4 and 5) that are not easily explained, but that may be artefacts arising from partially submerged electrodes or electrodes located at the saturated-unsaturated interface, which can cause problems for inversion. There are also increases in ρ_{1D} and ρ_{3D} observed at the top of shale (Figures 2 and 4) that may be due to the occurrence of increased gravel or till not represented by the major lithological contacts (e.g., Crow et al., 2020).

The unsaturated zone appears chargeable to a significant extent for all boreholes (Figures 2–5), possibly due to the predominance of capillary-bound water. Also chargeable are the gravels, but to a lesser extent, possibly indicative of increased interconnected surface area (e.g., Slater, 2007) or clay content associated with the presence of a basal till layer not recorded in the drill logs, but interpreted from geophysical data (Crow et al., 2020). There appears to be some occurrences of more chargeable material within the clay silt, which might imply increased surface area, but that cannot be correlated to any particular lithology. The records indicate high normalized chargeability for the shale, but given the high degree of misfit for the chargeability inversions and the depths of investigation, chargeability of the shale is subject to significant uncertainty.

The frequency distributions of the different resistivity records for each lithology are shown in Figure 7. The resistivity records exhibit distributions that reflect the similarities observed in the logs and pseudo-logs. In particular, sand or sand and gravel are mostly separable from clay-silt, but less so from shale. Conversely, sand and gravel is largely indistinguishable from sand alone. The different lithologies (particularly sand and gravel combined) are most separable for the 1D resistivity logs ρ_a and ρ_{1D} that do not involve inversion for resistivity (Figure 7a, b). The resistivity distributions for the pseudo-logs of ρ_{2D} and ρ_{3D} exhibit more overlap between

lithologies (Figure 7c, d). This result is expected for records arising from smoothness-constrained inversion, whereby resistivity must transition across contacts. The practical implication is that high-fidelity lithological prediction may be difficult based on resistivity alone, particularly for the surface-based surveys (ρ_{2D}).

Lithology of the aquifer system appears to be more separable in terms of resistivity than in terms of 1D or 3D normalized chargeability (Figure 8). Although high normalized chargeability can be used to predict clay silt or shale with some confidence, low normalized chargeability cannot be used to confidently discriminate any particular lithology beyond the exclusion of shale or unsaturated sediments. Unlike for resistivity, the 1D normalized integral chargeability M_n does not show significantly more separability than the 3D normalized intrinsic chargeability m_n that results from inversion.

Hydraulic Conductivity

The lithological control on the available hydraulic conductivity measurements is illustrated in Figure 9. Sand exhibits a large range of hydraulic conductivity with some low conductivity measurements attributed to the variable presence of silt within the sandy esker carapace. Nevertheless, the lithology of clay silt is largely separable from sand or sand and gravel in terms of hydraulic conductivity. In contrast, the hydraulic conductivity for sand and gravel is completely contained within the distribution for sand, thereby rendering sand and gravel indistinguishable from sand (similar to the results for resistivity). It is then largely the distinction between clay silt (aquitard) and sand or sand and gravel (aquifer) that is most important from a hydrogeological perspective within the Quaternary aquifer system (excluding the bedrock aquiclude for which there are no measurements of hydraulic conductivity). This classification is best achieved with the resistivity records of ρ_a or ρ_{1D} for which all but a few samples can be separated (Figure 7a, b) and, to a lesser extent, ρ_{3D} (Figure 7d). In all cases, occurrences of shale (for which hydraulic conductivity is unknown) may be incorrectly identified as sand or sand and gravel based on resistivity without additional information. A distinction of aquitard versus aquifer cannot be achieved with chargeability records alone due to the limited separability (Figure 8).

The correlation between electrical resistivity and hydraulic conductivity is illustrated in Figure 10. The strongest correlation is observed for ρ_{1D} and ρ_a, even more so than for lithology (although lithology is represented as a simple ordinal variable that may be insufficient to capture covariance). Figure 11 illustrates the simple predictive capability of resistivity for hydraulic

conductivity using the records of ρ_{1D} and ρ_{2D} for comparison. The data are fit with a power law relationship for which a relative change in resistivity results in a proportional relative change in hydraulic conductivity according to a log-log linear equation of the form

$$\log(K_h) = \alpha \log(\rho) + \log(b) \;\Rightarrow\; K_h = b\,\rho^{\alpha} \quad (4)$$

for which the positive exponent α indicates increased K with increased ρ due to an increase in fresh water-saturated pore volume. Mean prediction error is approximately one-half an order of magnitude of hydraulic conductivity using ρ_{1D} and just less than two-thirds an order of magnitude of hydraulic conductivity using $\rho_{2D.}$ This level of accuracy is comparable to other hydrogeophysical predictive models for hydraulic conductivity (e.g., Glaser, 2021). Prediction errors can be lowered slightly by considering clay silt samples independently from sand or sand and gravel samples, but this is only possible given lithological records and separable resistivity distributions, which is not the case for ρ_{2D}.

Petrophysical Modelling

Petrophysical modelling was performed using samples from boreholes 1, 2 and 4 for which borehole fluid conductivity and NMR porosity were measured. Samples for saturated clay silt were isolated, but samples for sand were combined with those of sand and gravel (hereafter refereed to as sand and gravel) due to the observed overlap in terms of lithology and hydraulic conductivity, and due to the limited number of sand and gravel samples. No attempt was made to model the unsaturated sediments or the shale for which measurements are limited. Petrophysical modelling results are illustrated in Figure 12 for the 1D apparent resistivity log ρ_{1D}. The other resistivity records exhibit similar behaviour as expected from the high degree of correlation between the records (Figure 6a) and results of fitting petrophysical model parameters to all records are summarized in Table 1.

In general, the data do not depict clear Archie-type trends with fluid conductivity as per equation (1). The data exhibit clustering of samples from each borehole for which the fluid conductivity is nearly constant (Figure 12a, b). The sand and gravel measurements from BH1 are an exception to the clustering behaviour, but still do not exhibit a clear Archie-type trend (Figure 12b). This behaviour is also reflected in the sample-based estimates of F (Figure 12c, d) and the sample-based estimates of c using equation (2) with total porosity and $a = 1$ (Figure 12e, f). The sample-based estimates are clustered and have large standard deviations (Table 1). Attempts at using mobile porosity, or the sum of mobile and capillary porosity in equation (2) resulted in values of c less than unity, which is only possible in the case of unaccounted for surface conductivity. Attempts to estimate c using equation (3) were unsuccessful, yielding weak

correlation, p-values greater than 0.05, large values of a, and values of c less than unity. Attempts at nonlinear fitting of equation (1) resulted in poor fits, but yielded a range of porosity exponents from 2–5 for clay silt and 2–2.5 for sand and gravel with corresponding surface conductivities of approximately 10 mS/m and 5 mS/m.

DISCUSSION

The borehole electrical resistivity records for the Vars-Winchester esker aquifer convey similar lithological information, but exhibit significant differences in resistivity. At another Champlain Sea site near Ottawa, a consistent factor of two difference is observed between EM39 measurements and 2D resistivity pseudo-logs (Crow et al., 2017). Similar discrepancies are observed at other sites between EM39 measurements and 2D resistivity pseudo-logs, but with less consistency (Aubrey, 2010; Hermans et al., 2011; Robert et al., 2012; Caterina et al. 2014). In some cases, there is a near 1:1 correspondence between ρ_a and ρ_{2D} (Aubry, 2010; Hermans et al., 2011) and in other cases, the differences are near an order of magnitude (Caterina et al., 2014). In contrast, Maurer et al. (2009) demonstrate a very good match between borehole induction logs and 2D resistivity pseudo-logs with the important distinction being that their study creates pseudo-logs from inversion of down-hole galvanic electrical data.

It is well known that the low induction number approximation used for EM39 measurements is only valid for resistive environments (McNeil, 1980). For environments with resistivity less than approximately 10 Ωm, the EM39 reported measurement is an overestimation of the true resistivity (McNeil, 1986). For the Vars-Winchester esker aquifer, observed resistivity is less than 10 Ωm for the clay silt (Figure 6a). However, correction to lower resistivity would not significantly alter the results since only a small number of samples would be corrected, and uncorrected ρ_a is already consistently less than the other measures of resistivity. Furthermore, discrepancies exist among the galvanic resistivity records themselves, indicating that different measurement physics alone cannot account for observed differences.

The largest source of inconsistency between the different resistivity records is likely the differences in scale of the respective volumes of investigation or the sensitivity distributions (e.g., Christensen and Lawrie, 2018). Even with physically-based inversion of galvanic resistance measurements to recover electrical resistivity at arbitrarily small scales, the measurements are not necessarily sensitive to that level of detail. It might be expected that any resistivity record with a volume of investigation approaching that of the EM39 would demonstrate a greater degree of similarity. Indeed, the 3D resistivity pseudo-log is most similar

to the EM39 log in terms of resistivity, although the correlation is slightly stronger for the 1D log. The 1D borehole apparent conductivity measurements have a volume of investigation similar to the 3D surface-to-borehole survey. However, the surface-to-borehole measurements involve multiple measurements and quadrupole combinations that result in higher sensitivity, and the measurements are then inverted which is a form of sensitivity focusing.

Similarly, the results of an EM39 log can be explained by any reasonable distribution of near-borehole anomalies that are large relative to the EM39 volume of investigation, but small relative the 1D, 2D, or 3D volumes of investigation (Christensen and Lawrie, 2018). This is particularity relevant considering the fact that borehole installation typically creates a zone of disturbance around the borehole itself. Borehole effects illustrate the situation that some inconsistencies may or may not be relevant to the problem of large-scale aquifer characterization. For example, the elevated resistivity ρ_{2D} between approximately 55–65 m elevation observed for BH1 to BH3 is not nearly as well resolved in EM39, 1D, or 3D records, but is highly aligned with a prominent seismic reflector observed laterally across the esker aquifer system (Pugin et al., 2009). Although the ρ_{2D} pseudo-log appears to be least representative of the immediate near-borehole environment based on consistency with other records, it may be a better representation of the larger-scale aquifer system.

Another source of inconsistency is anisotropy. The theoretical current flow for the EM39 is purely horizontal and the measurements are indicative of the horizontal resistivity ρ_h. In contrast, the current flow for the galvanic resistivity surveys is multi-directional (radial about an electrode) such that the measurements are indicative of the bulk resistivity ρ_b. Horizontal and bulk resistivity are the same for isotropic media, but not for anisotropic media with either micro-anisotropy (below the measurement scale) or macro-anisotropy (resulting from resolvable layering). The bulk resistivity and the factor of anisotropy κ are related by

$$\rho_b = \sqrt{\rho_v \, \rho_h} \;\Rightarrow\; \kappa = \sqrt{\rho_v / \rho_h} = \rho_b / \rho_h \approx \rho_{1D,2D,3D} / \rho_a \qquad (5)$$

where ρ_v is the vertical resistivity (e.g., Christensen, 2000). The resistivity records indicate a factor of anisotropy of approximately 2–4 (Figure 6a). However, since the galvanic resistivity records exhibit discrepancy among themselves, the difference between the EM39 and the 2D pseudo-log cannot be entirely attributed to anisotropy. At most, the factor of anisotropy is approximately 2, which seems reasonable (e.g., Christensen, 2000) and is also observed in nearby settings (Crow et al., 2017). The remaining discrepancy between ρ_{2D} and the other resistivity records must be attributed to differences in scale.

It is also important to note that the preceding comparisons involve both data (ρ_a, ρ_{1D}) and model space (ρ_{2D}, ρ_{3D}). This can be remedied by forward modelling results from the electrical resistivity surveys into the data space of the EM39, or by inverting the EM39 or 1D apparent conductivity. This might be a necessary approach for calibration efforts (e.g., Foged et al., 2013) but given the high measurement density of the EM39 and the overwhelming scale effects, it can likely be considered to be of secondary concern. Christensen and Lawrie (2018) show that the model recovered from formal inversion of high-resolution inductive log data is a reasonable approximation to simple averaging of the apparent conductivity. They also note that the presumably innocuous procedure of averaging is in essence a model formulation for which the accepted sensitivity function is equivalent to the chosen averaging filter.

The estimates of surface conductivity from 0–32 mS/m (Table 1) are lower than expected for Champlain Sea sediments (e.g., Hyde and Hunter, 1998; Aubrey, 2010). Using normalized chargeability to estimate the variable surface conductivity results in even lower estimates of surface conductivity that are independent of the resistivity record: less than 2.5 mS/m for clay silt and less than 1 mS/m for sand or sand and gravel (Figure 13). The discrepancy is partly due to a scaling difference between the time-integrated normalized chargeability measured for the surveys considered herein, and the Cole-Cole chargeability utilized by Weller et al. (2013). Regardless, the variable estimates of surface conductivity exhibit an increase with depth for the clay silt that may be useful in interpreting the degree of leaching associated with Champlain Sea sediments (Figure 8a)

The apparent underestimation of surface conductivity and the poor petrophysical model performance are attributed to borehole fluid conductivity measurements that are entirely in-hole and not representative of the pore fluid. Large values of a, and values of c less than unity are consistent with poor data quality and inadequate representation of surface conduction (Glover, 2015). The results of the petrophysical modelling cannot likely be used for predictive purposes.

CONCLUSION

Electrical resistivity and induced polarization survey results for the Vars-Winchester esker aquifer system can be interpreted in terms of borehole geophysical logs, observations of lithology, and hydraulic conductivity. The galvanic resistivity logs and pseudo-logs are in nominal agreement with EM39 induction logs of apparent resistivity, but there are significant differences in resistivity values. Some of the discrepancy is likely a result of scale differences, while some of the discrepancy is attributable to an anisotropy factor of approximately 2

associated with the different measurement geometries. Estimates of petrophysical model parameters and surface conductivity derived from Archie's Law are unreliable due to fluid conductivity measurements that do no represent the pore fluid. Borehole logs and pseudo-logs recovered from the 1D, 2D, and 3D surveys all exhibit some degree of separability in terms of lithology that can be used to distinguish between aquifer (sand and sand and gravel) or aquitard (clay silt) for the aquifer system. The resistivity records also exhibit significant correlation with hydraulic conductivity that can be used for prediction away from boreholes. For the Vars-Winchester esker aquifer, chargeability is less useful than resistivity for lithological characterization or prediction of hydraulic conductivity. It may be useful as part of a multiple linear regression or machine learning approach.

The largest discrepancy between all resistivity records is observed for the pseudo-logs derived from the 2D surface surveys. These surveys have the largest volume of investigation for all of the measurements considered along with the lowest resolution for the resistivity inversions. As such, they are the least separable in terms of lithology, and the least accurate for prediction of hydraulic conductivity. Nevertheless, it is precisely these surveys that are most commonly used for hydrogeophysical applications as they offer high degrees of lateral coverage without the need for borehole electrodes. Caution is required when calibrating 2D resistivity surveys against other measures of resistivity, including borehole electromagnetic induction measurements. In some cases, borehole records may not represent a suitable "ground-truth" for validating surface surveys unless differences of geometry and scale can be accounted for.

ACKNOWLEDGEMENTS

This work is part of the Natural Resources Canada Groundwater Geoscience Program. Field data acquisition assistance by K. Brewer, T. Cartwright, B. Dietiker, and M. Griffiths. Geophysical logs and information provided by H. Crow. Land access provided by A. Brisson, R. Bordeau, and the South Nation Conservation Authority. Internal review by H. Crow. Raw and processed data and models are available from the author under the Open Government Licence – Canada. https://open.canada.ca/en/open-government-licence-canada

REFERENCES

Aubry, K.A.-M., 2010. Predicting sensitive and quick clays using electrical and electromagnetic geophysical methods in Champlain Sea sediments, Ottawa, Canada. B.Sc. Thesis, Carelton University.

Caterina, D., Hermans, T., Nguyen, F., 2014. Case studies of incorporation of prior information in electrical resistivity tomography: comparison of different approaches. Near Surface Geophysics 12, 451–465. https://doi.org/10.3997/1873-0604.2013070

Christensen, N.B., 2000. Difficulties in determining electrical anisotropy in subsurface investigations. Geophysical Prospecting 48, 1–19. https://doi.org/10.1046/j.1365-2478.2000.00174.x

Christensen, N.B., Lawrie, K.C., 2018. A novel approach to comparing AEM inversion results with borehole conductivity logs. Exploration Geophysics 49, 309–322. https://doi.org/10.1071/EG17029

Crow, H., Alpay, S., Hinton, M., Knight, R., Oldenborger, G., Percival, J.B., Pugin, A.J.-M., Pelchat P., 2017. Geophysical, geotechnical, geochemical, and mineralogical data sets collected in Champlain Sea sediments in the Municipality of Pontiac, Quebec. Geological Survey of Canada, Open File 7881. https://doi.org/10.4095/301664

Crow, H.L., Pugin, A.J.-M., Dietiker, B., Paradis, D., Brewer, K., Cartwright, T., Griffiths, M., Russell, H.A.J., 2020. Lithological and hydrogeological properties from a downhole geophysical dataset in the Vars-Winchester esker, Ontario. Geological Survey of Canada, Open File 8536, 147–158. https://doi.org/10.4095/321078

Crow, H., Paradis, D., Grunewald, E., Liang, X.X., Russell, H.A.J., 2022. Hydraulic Conductivity from Nuclear Magnetic Resonance Logs in Sediments with Elevated Magnetic Susceptibilities. Groundwater. https://doi.org/10.1111/gwat.13158

Cummings, D.I., Gorrell, G., Guilbault, J.-P., Hunter, J.A., Logan, C., Ponomarenko, D., Pugin, A.J.-M., Pullan, S.E., Russell, H.A.J., Sharpe, D.R., 2011. Sequence stratigraphy of a glaciated basin fill with a focus on esker sedimentation. GSA Bulletin 123, 1478–1496. https://doi.org/10.1130/B30273.1

Cummings, D.I., Russell, H.A.J., 2007. The Vars-Winchester esker aquifer, South Nation River watershed, Ontario. Geological Survey of Canada, Open File 5624. https://doi.org/10.4095/224424

Edwards, L.S., 1977. A modified pseudosection for resistivity and IP. Geophysics, 42, 1020–1036. https://doi.org/10.1190/1.1440762

Foged, N., Auken, E., Christiansen, A.V., Sørensen, K.I., 2013. Test-site calibration and validation of airborne and ground-based TEM systems. Geophysics 78, E95–E106. https://doi.org/10.1190/geo2012-0244.1

Glaser, D.R., 2021. A Site-specific Comparison of Permeability Prediction Models in Alluvial Sediments from Physical and Geoelectrical Measurements. Journal of Environmental and Engineering Geophysics 26, 315–322. https://doi.org/10.32389/JEEG21-025

Glover, P.W.J., 2015. Geophysical Properties of the Near Surface Earth: Electrical Properties. Treatise on Geophysics (Second Edition), 89–137. https://doi.org/10.1016/B978-0-444-53802-4.00189-5

Glover, P.W.J., 2016. Archie's law – a reappraisal. Solid Earth 7, 1157–1169. https://doi.org/10.5194/se-7-1157-2016

Hermans, T, Daoudi, M., Vandenbohede, A., Robert, T., Caterina, D., Nguyen, F., 2012. Comparison of temperature estimates from heat transport model and electrical resistivity tomography during a shallow heat injection and storage experiment. Berichte der Geologischen Bundesanstalt 93, 43–48. https://www.geologie.ac.at

Hyde, C.S.B., Hunter, J.A., 1998. Formation electrical conductivity-porewater salinity relationships in Quaternary sediments from two Canadian sites. Symposium on the Application of Geophysics to Environmental and Engineering Problems, 499–510. https://doi.org/10.3997/2214-4609-pdb.203.1998_053

Maurer, H., Friedel, S., Jaeggi, D., 2009. Characterization of a coastal aquifer using seismic and geoelectric borehole methods. Near Surface Geophysics 7, 353–366. https://doi.org/10.3997/1873-0604.2009014

McNeil, J.D., 1980. Electromagnetic terrain conductivity measurements at low induction numbers. Geonics Ltd., Technical Note TN-6. http://www.geonics.com

McNeil, J.D., 1986. Geonics EM39 borehole conductivity meter: Theory of operation. Geonics Ltd., Technical Note TN-20. http://www.geonics.com

Oldenborger, G.A., 2021. Electrical resistivity surveys, Vars-Winchester esker aquifer, Ontario. Geological Survey of Canada, Open File 8769. https://doi.org/10.4095/328037

Oldenborger, G.A., Knoll, M.D., Routh, P.S., LaBrecque, D.J., 2007. Time-lapse ERT monitoring of an injection/withdrawal experiment in a shallow unconfined aquifer. Geophysics 72, F177–F187. https://doi.org/10.1190/1.2734365

Oldenborger, G.A., Pugin, A.J.-M., Pullan, S.E., 2013. Airborne time-domain electromagnetics, electrical resistivity and seismic reflection for regional three-dimensional mapping and characterization of the Spiritwood Valley Aquifer, Manitoba, Canada. Near Surface Geophysics 11, 63–74. https://doi.org/10.4095/328037

Oldenborger, G.A., Routh, P.S., 2009. The point-spread function measure of resolution for the 3-D electrical resistivity experiment. Geophysical Journal International 176, 405–414. https://doi.org/10.1111/j.1365-246X.2008.04003.x

Paradis, D., Pugin, A., Crow, H., Oldenborger, G., Russell, H., Melaney, M., 2020. Hydrogeophysics for the characterization of hydraulic properties of a buried esker system: An overview. Geological Survey of Canada, Open File 8536, 131–138. https://doi.org/10.4095/321078

Pugin, A.J.-M., Pullan, S.E., Hunter, J.A., Oldenborger, G.A., 2009. Hydrogeological prospecting using P- and S-wave landstreamer seismic reflection methods. Near Surface Geophysics 7, 315–327. https://doi.org/10.3997/1873-0604.2009033

Revil, A., Coperey, A., Shao, Z., Florsch, N., Fabricius, I.L., Deng, Y., Delsman, J.R., Pauw, P.S., Karaoulis, M., de Louw, P.G.B., van Baaren, E.S., Dabekaussen, W., Menkovic, A., Gunnink, J.L., 2017. Complex conductivity of soils. Water Resources Research 53, 7121–7147. https://doi.org/10.1002/2017WR020655

Robert, T., Caterina, D., Deceuster, J., Kaufmann, O., Nguyen, F., 2012. A salt tracer test monitored with surface ERT to detect preferential flow and transport paths in fractured/karstified limestones. Geophysics 77, B55–B67. https://doi.org/10.1190/geo2011-0313.1

Sapia, V., Oldenborger, G.A., Jørgensen, F., Marchetti, M., Viezzoli, A., Pugin, A., 2015. 3D modeling of buried valley geology using airborne electromagnetic data. Interpretation 3, SAC9–SAC22. https://doi.org/10.1190/INT-2015-0083.1

Sauriol, J., 2016. Provenance of buried esker groundwater: the case of Vars-Winchester esker aquifer, Eastern Ontario, Canada. Hydrogeology Journal 24, 123–139. https://doi.org/10.1007/s10040-015-1327-1

Siemon, B., Christiansen, A.V., Auken, E., 2009. A review of helicopter-borne electromagnetic methods for groundwater exploration. Near Surface Geophysics 7, 629–646. https://doi.org/10.3997/1873-0604.2009043

Slater, L., 2007. Near surface electrical characterization of hydraulic conductivity: From petrophysical properties to aquifer geometries—A review. Surveys in Geophysics 28, 169–197. https://doi.org/10.1007/s10712-007-9022-y

Steuer, A., Siemon, B., Auken, E., 2009. A comparison of helicopter-borne electromagnetics in frequency- and time-domain at the Cuxhaven valley in Northern Germany. Journal of Applied Geophysics 67, 194–205. https://doi.org/10.1016/j.jappgeo.2007.07.001

Torrance, J.K., 1983. Towards a general model of quick clay development. Sedimentology 30, 547–555. https://doi.org/10.1111/j.1365-3091.1984.tb01822.x

Weller, A., Slater, L., Binley, A., Nordsiek, S., Xu, S., 2015. Permeability prediction based on induced polarization: Insights from measurements on sandstone and unconsolidated samples spanning a wide permeability range. Geophysics 80, D161–D173. https://doi.org/10.1190/geo2014-0368.1

Weller, A., Slater, L., Nordsiek, S., 2013. On the relationship between induced polarization and surface conductivity: Implications for petrophysical interpretation of electrical measurements. Geophysics 78, D315–D325. https://doi.org/10.1190/geo2013-0076.1

TABLES

Table 1. Formation factor and cementation exponents calculated using different methodologies for different resistivity records for BH1, BH2, and BH4 combined. F and σ_s are determined from linear fits applied to σ_f vs. σ_T for each lithology. F_μ and c_μ are the arithmetic means of the sample-based values for each lithology calculated using σ_s, n, and $a = 1$ reported with uncertainty equal to one standard deviation. Arithmetic mean total porosity is 0.62 ± 0.11 for the clay silt, and 0.30 ± 0.09 for the sand and gravel.

	F	σ_s (mS/m)	F_μ	c_μ
Clay silt				
ρ_a	3.2	32.1	3.6 ± 1.8	2.6 ± 1.1
ρ_{1D}	3.3	9.9	4.7 ± 5.9	2.6 ± 1.0
ρ_{2D}	5.3	6.7	9.5 ± 9.8	4.3 ± 2.3
ρ_{3D}	1.5	0[1]	2.4 ± 0.2	1.4 ± 1.1
Sand and gravel				
ρ_a	4.4	4.8	4.6 ± 0.8	1.3 ± 0.4
ρ_{1D}	12.0	2.7	13.9 ± 5.3	2.2 ± 0.6
ρ_{2D}	5.4	0.0[1]	12.8 ± 9.0	1.9 ± 0.8
ρ_{3D}	4.8	0.0[1]	5.9 ± 2.3	1.4 ± 0.5

[1]negative intercept forced to zero

FIGURES

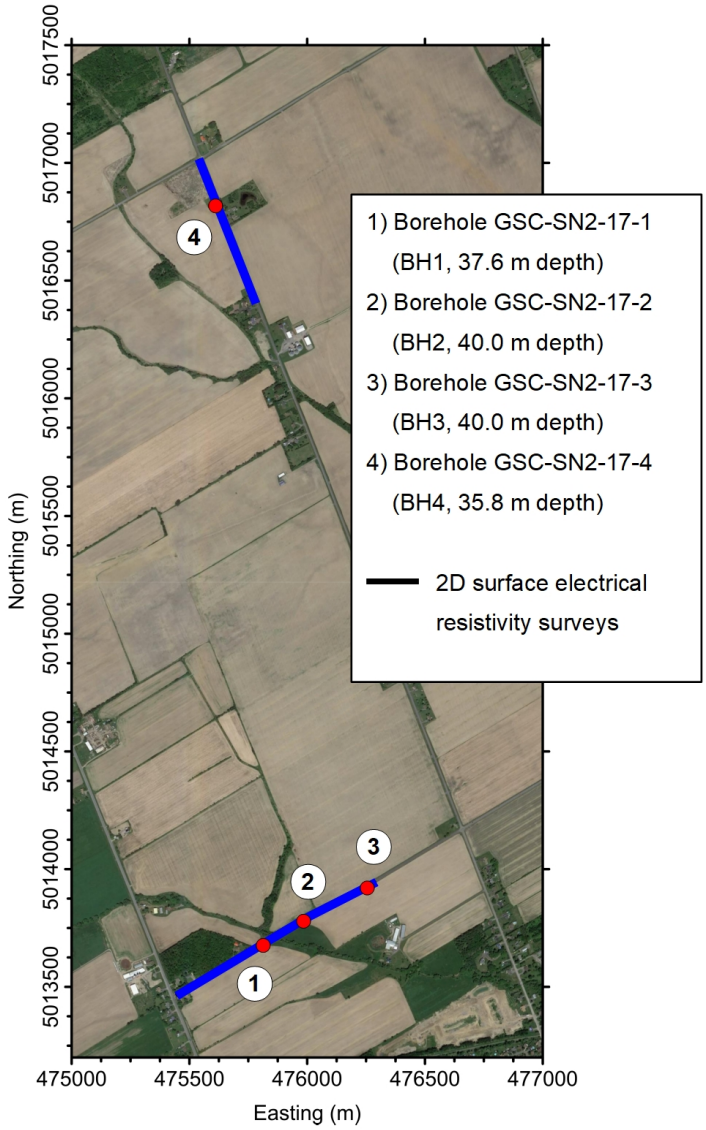

Figure 1. Study area showing locations of boreholes and the 2D surface electrical resistivity surveys. Map image: 01/06/2018, © 2020 Google.

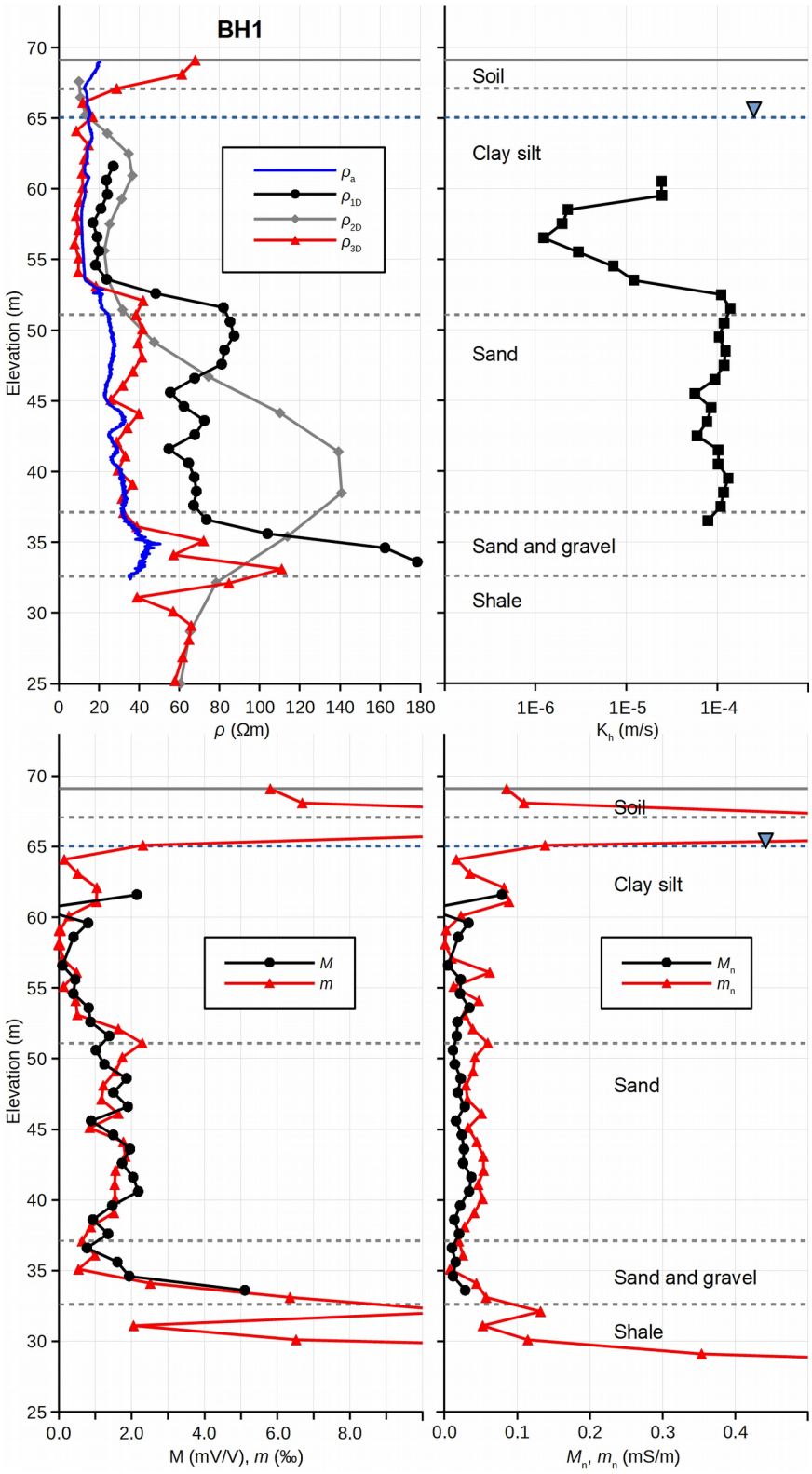

Figure 2. Electrical resistivity logs, pseudo-logs, and hydraulic conductivity log for BH1 with major lithostratigraphic contacts.

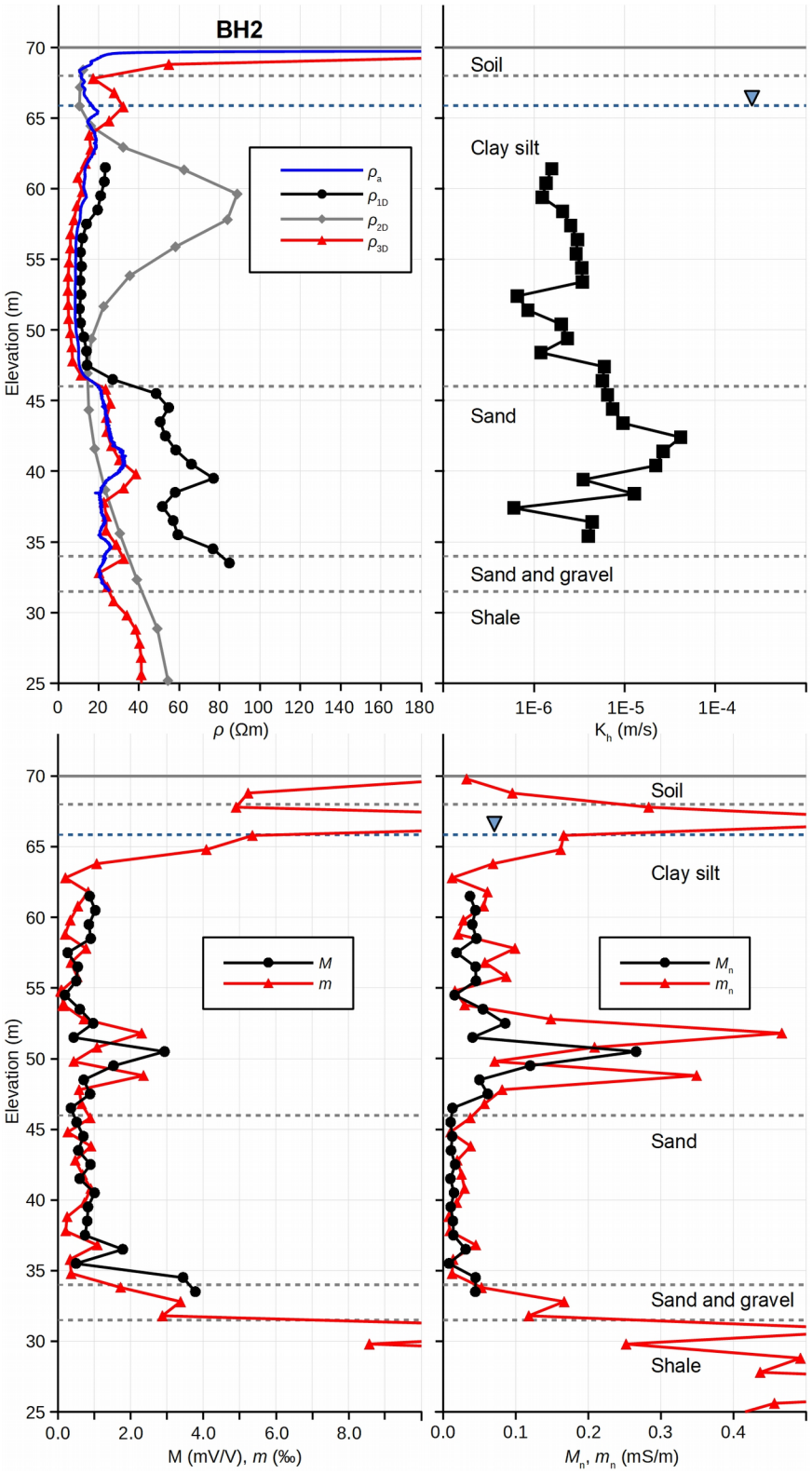

Figure 3. Electrical resistivity logs, pseudo-logs, and hydraulic conductivity log for BH2 with major lithostratigraphic contacts.

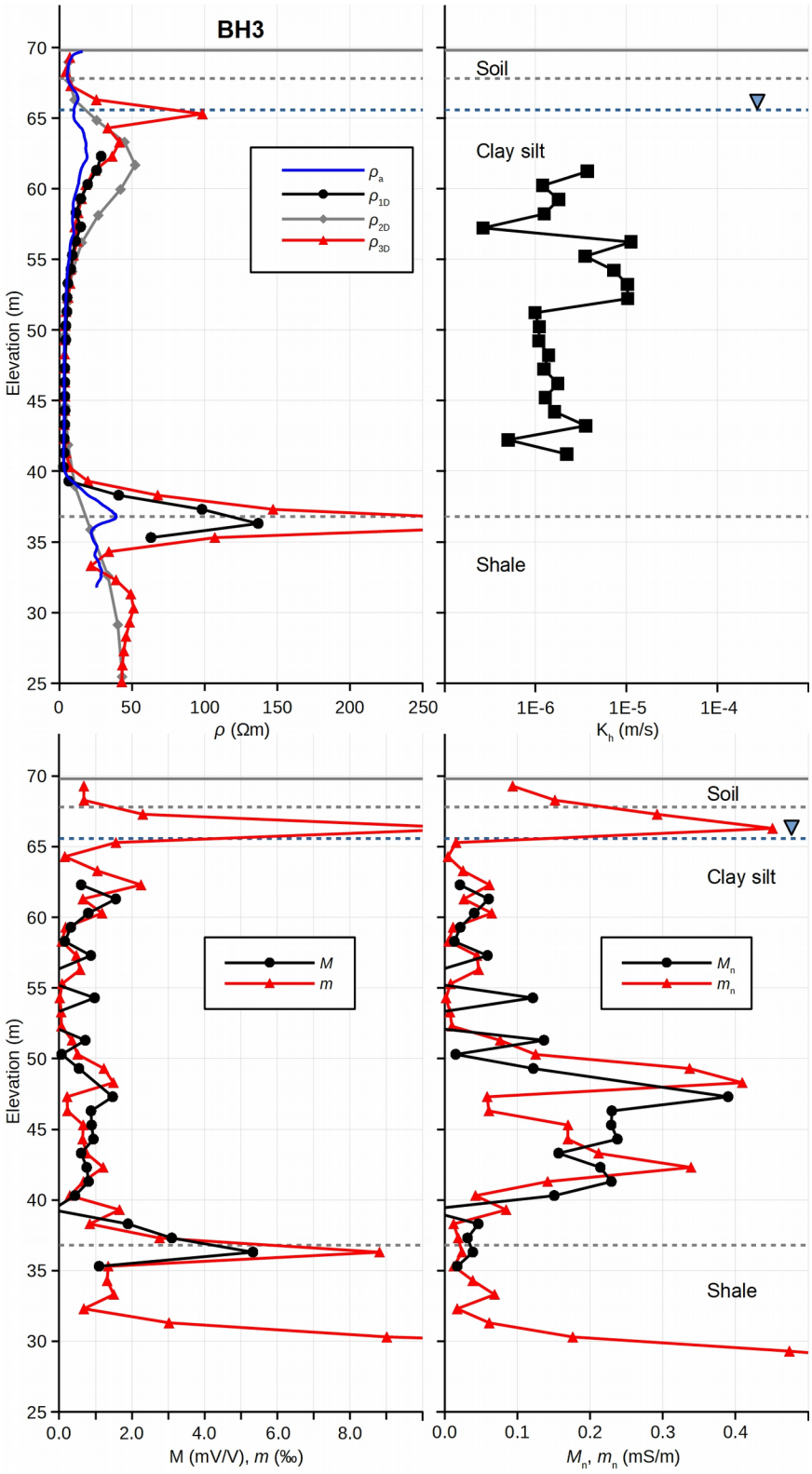

Figure 4. Electrical resistivity logs, pseudo-logs, and hydraulic conductivity log for BH3 with major lithostratigraphic contacts.

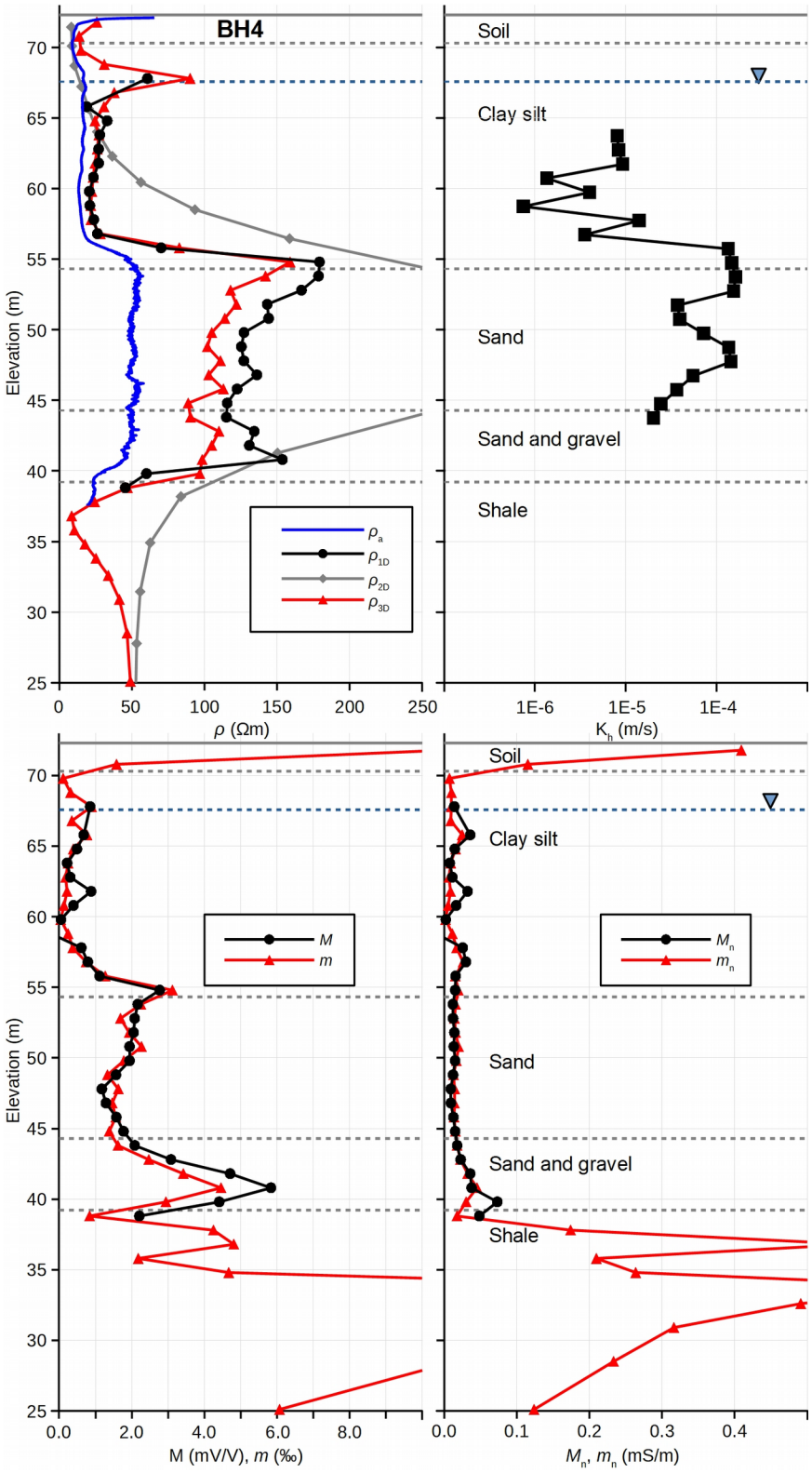

Figure 5. Electrical resistivity logs, pseudo-logs, and hydraulic conductivity log for BH4 with major lithostratigraphic contacts.

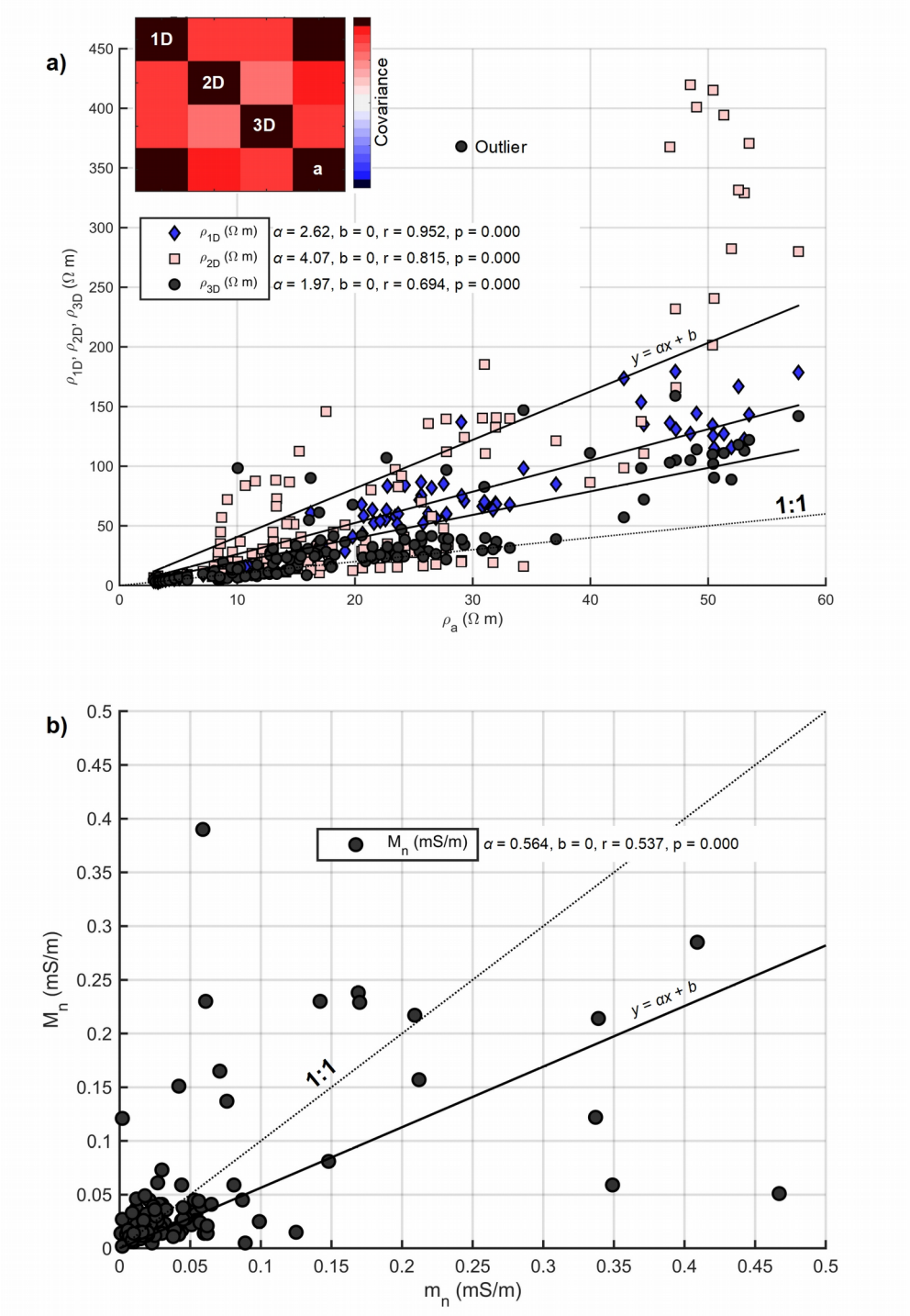

Figure 6. a) Point-based comparison of resistivity logs and pseudo-logs for all boreholes and lithologies. Inset shows the covariance matrix for the different resistivity records. b) Point-based comparison of normalized chargeability logs and pseudo-logs for all boreholes and lithologies. Parameters of the best-fitting linear model are displayed alongside the legends (intercepts are forced to zero).

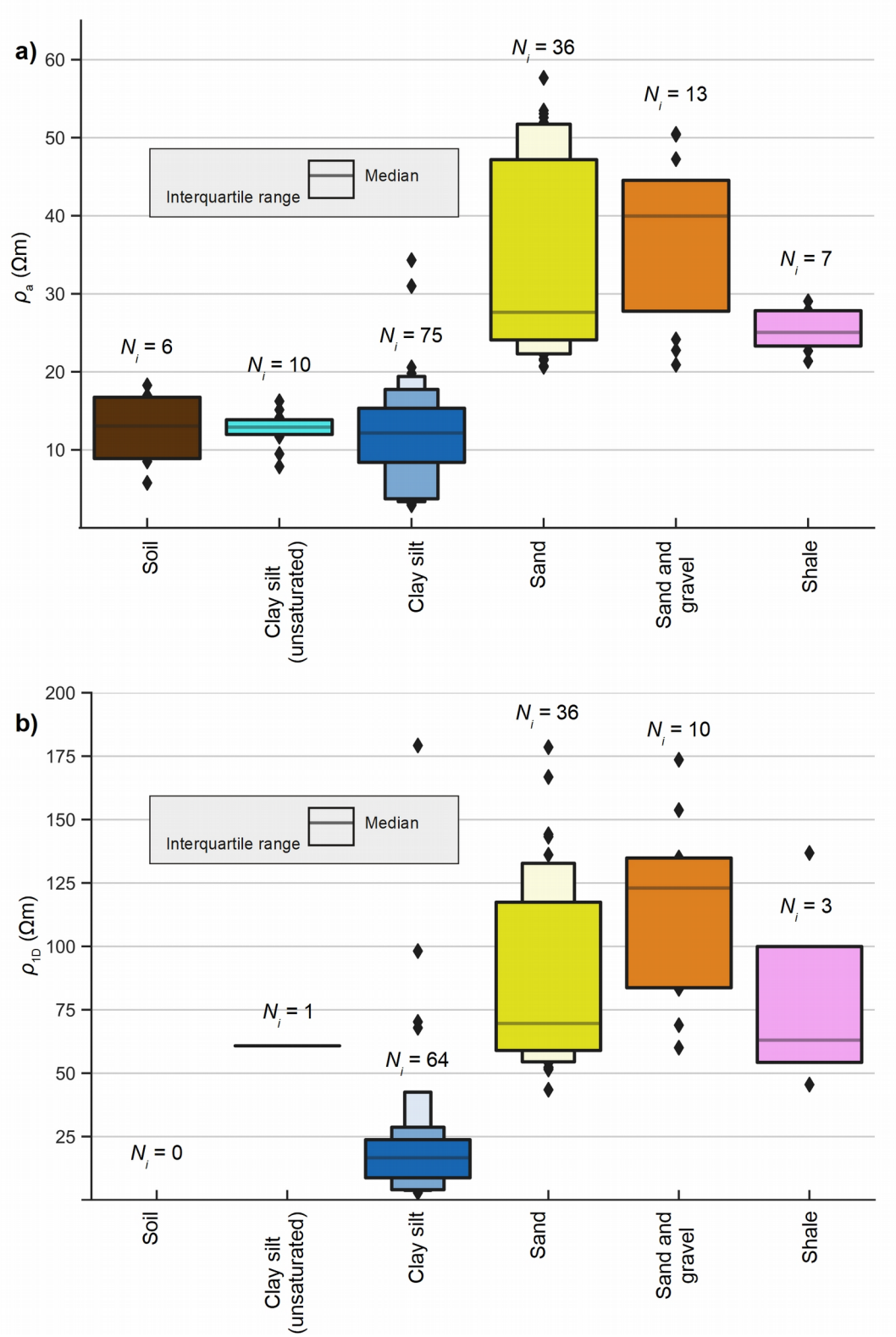
a)
ρ_a (Ωm)
60
50
40
30
20
10
Median
Interquartile range
N_i = 6
N_i = 10
N_i = 75
N_i = 36
N_i = 13
N_i = 7
Soil
Clay silt (unsaturated)
Clay silt
Sand
Sand and gravel
Shale
b)
ρ_{1D} (Ωm)
200
175
150
125
100
75
50
25
Median
Interquartile range
N_i = 0
N_i = 1
N_i = 64
N_i = 36
N_i = 10
N_i = 3
Soil
Clay silt (unsaturated)
Clay silt
Sand
Sand and gravel
Shale

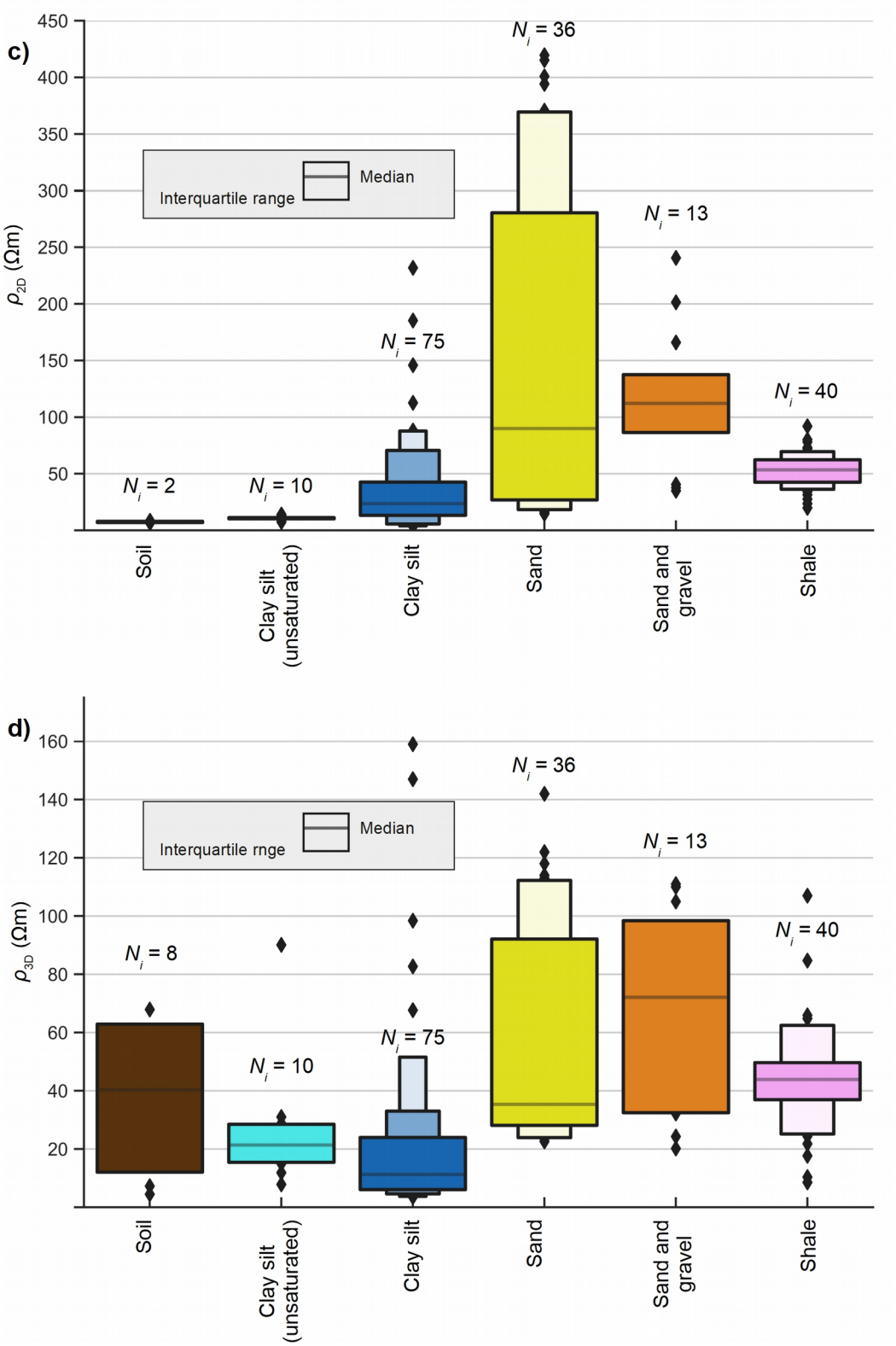

Figure 7. Frequency distribution of of resistivity for each lithology: a) ρ_a, b) ρ_{1D}, c) ρ_{2D}, and d) ρ_{3D}. The number of pairwise samples is given by N_i.

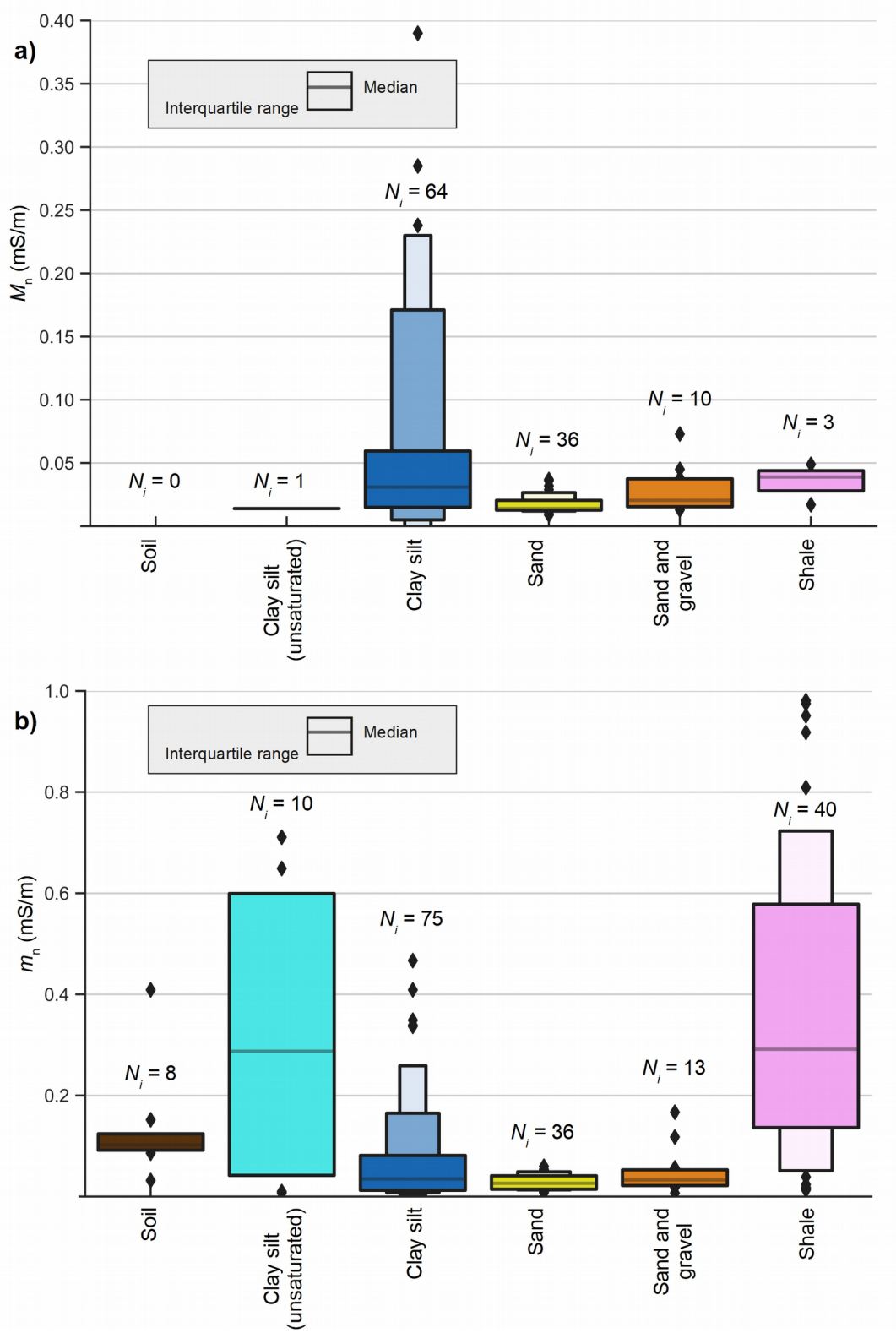

Figure 8. Frequency distribution of normalized chargeability for each lithology: a) M_n and b) m_n. The number of pairwise samples is given by N_i.

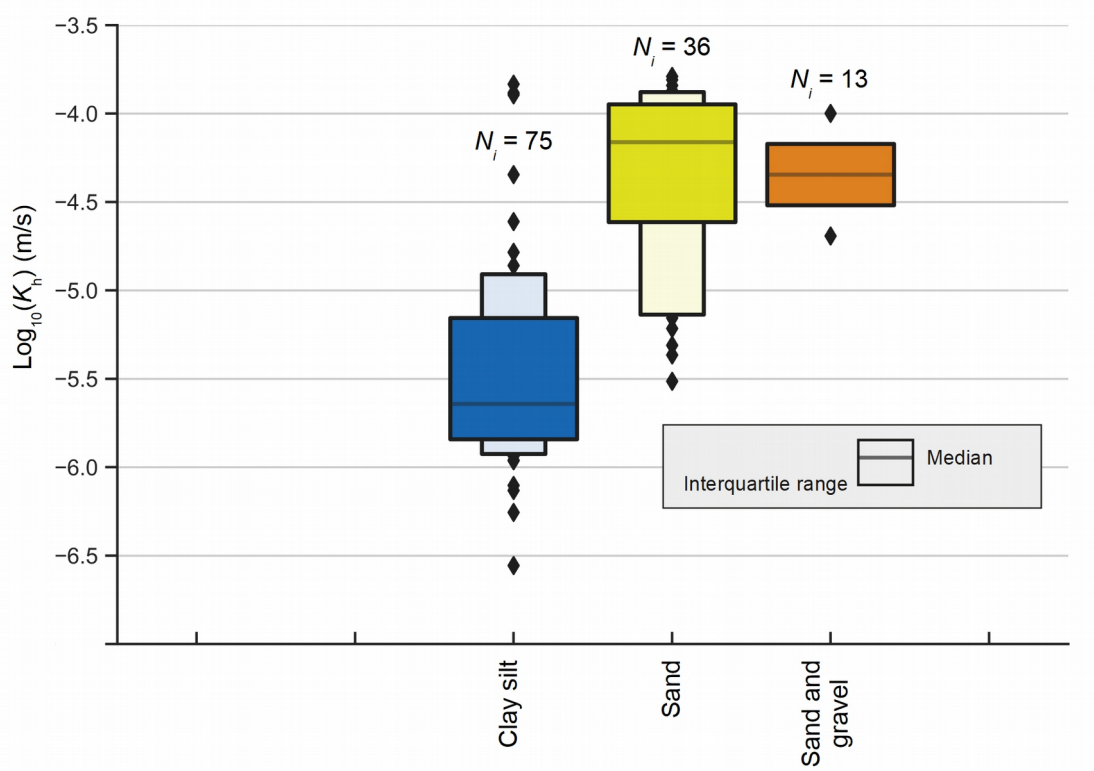

Figure 9. Frequency distribution of hydraulic conductivity for each lithology. The number of pairwise samples is given by N_i.

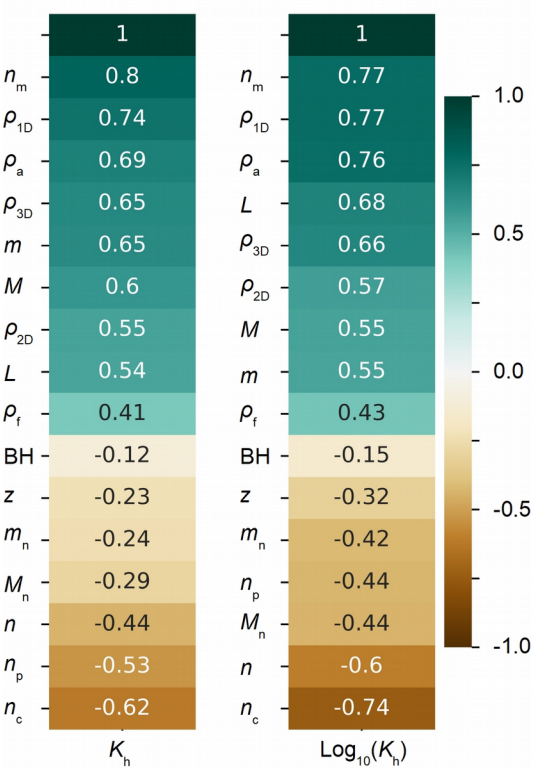

Figure 10. Pairwise correlation coefficients between hydraulic conductivity and the other borehole records. Co-linearity is possible. For example the larger correlation observed for chargeability versus normalized chargeability is likely due to co-linearity with resistivity that is removed during normalization.

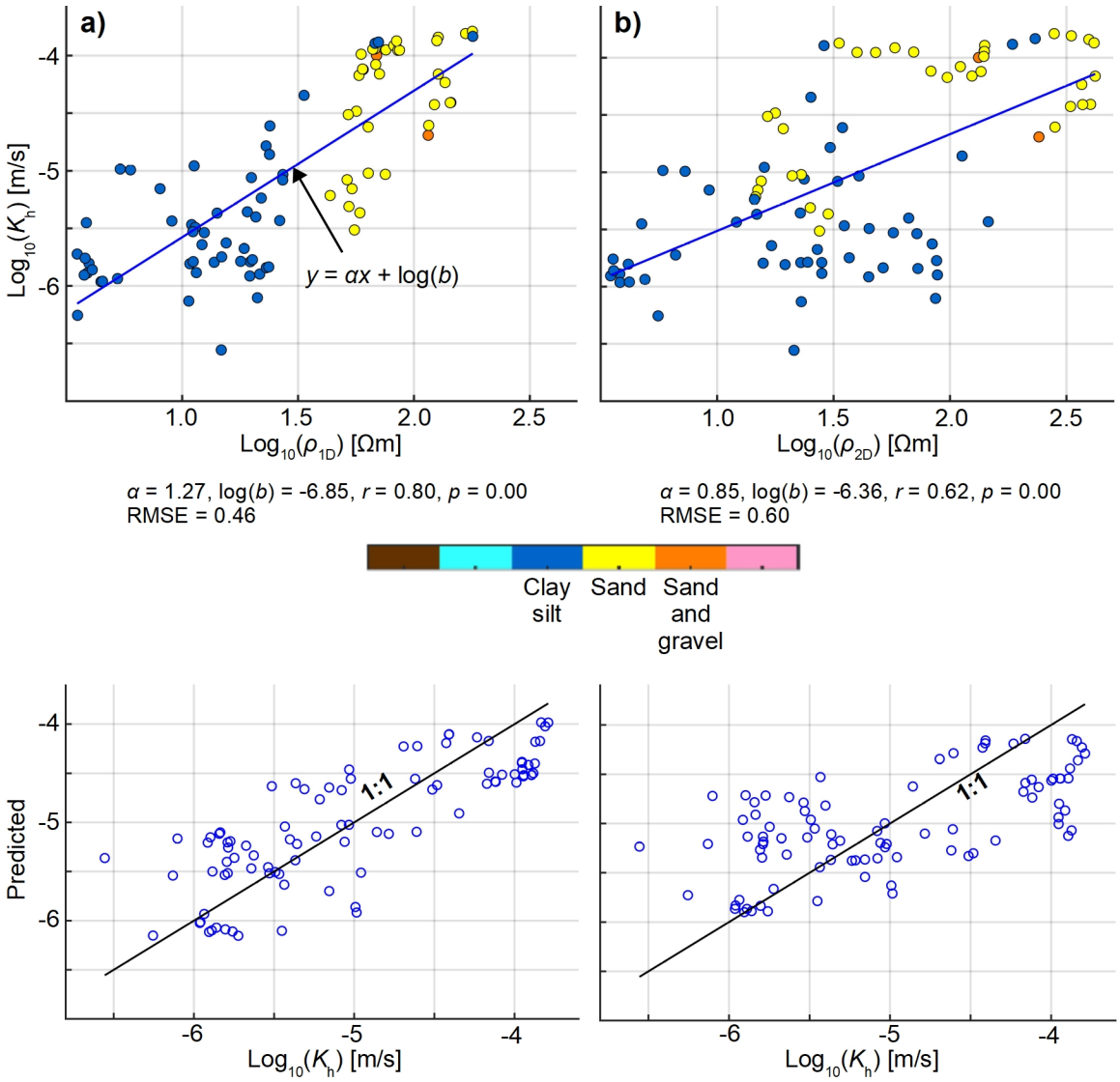

Figure 11. Predictive modelling of hydraulic conductivity using a) ρ_{1D} and b) ρ_{2D} for example.

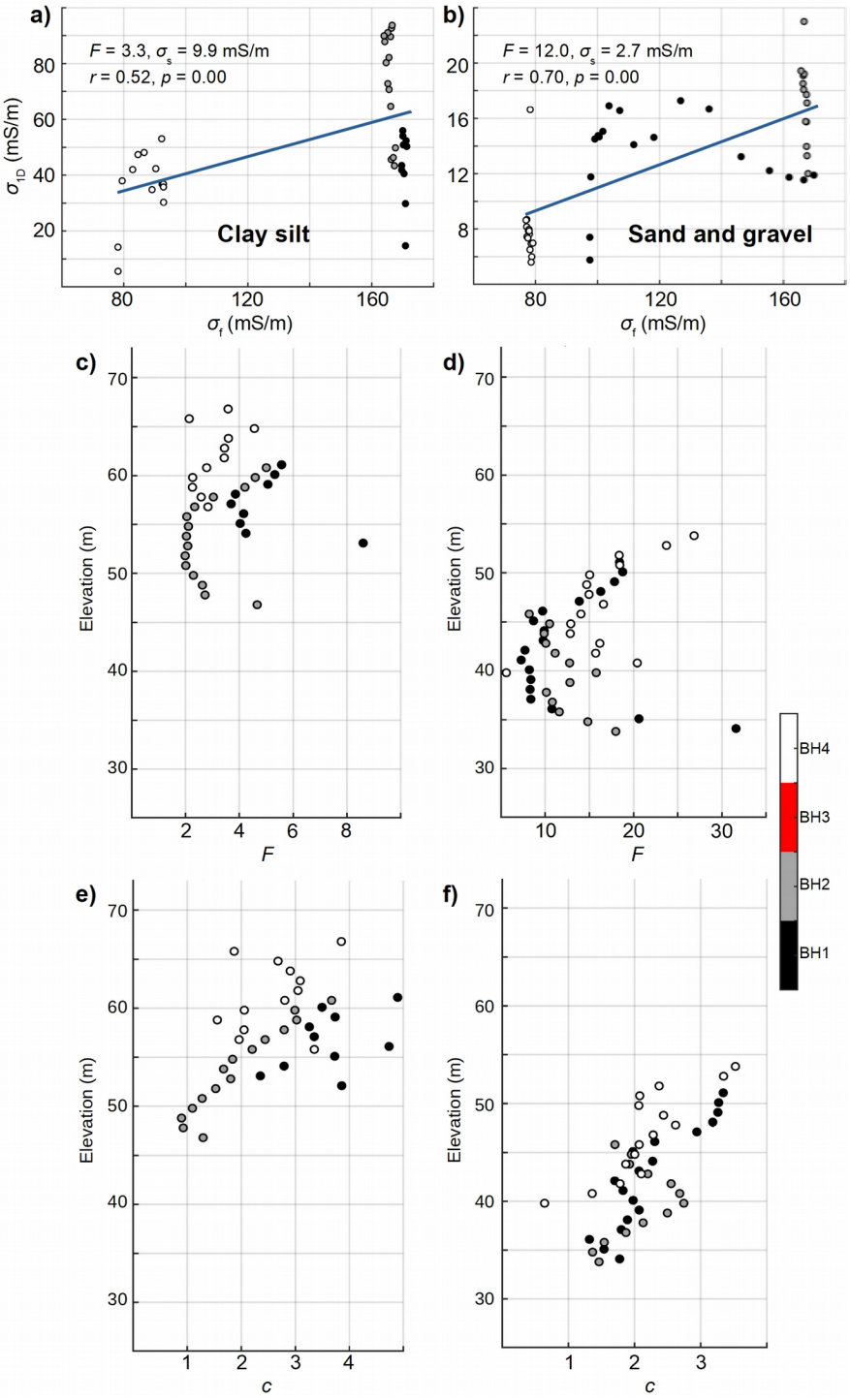

Figure 12. Petrophysical modelling of conductivity to determine formation factor and surface conductivity for a) clay silt and b) sand or sand and gravel. Sample-based estimates of formation factor for c) clay silt and d) sand or sand and gravel. Sample-based estimates of porosity exponent for e) clay silt and f) sand or sand and gravel. Fluid resistivity and porosity logs were not acquired for BH3.

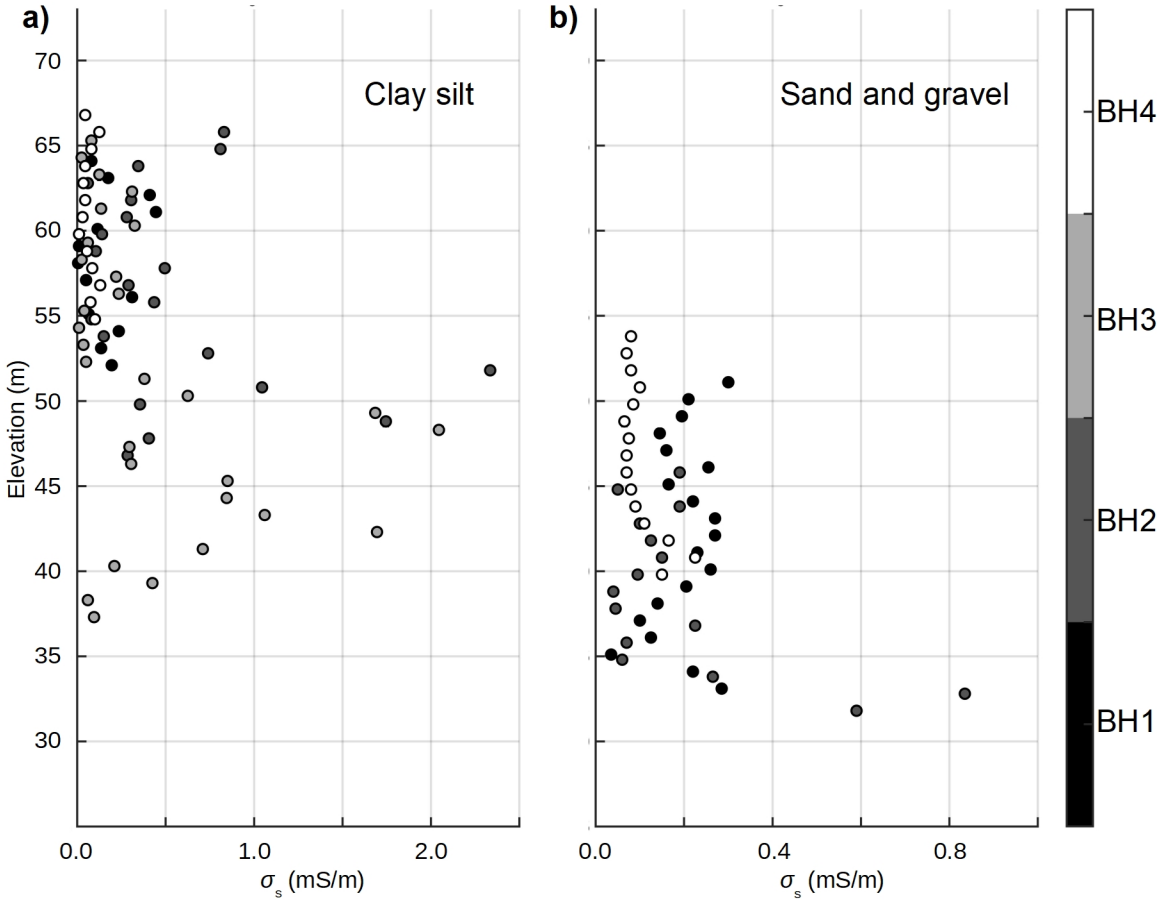

Figure 13. Sample-based surface conductivity estimated from normalized intrinsic chargeability m_n for a) clay silt and b) sand or sand and gravel.

APPENDIX

Borehole logs and pseudo-logs resampled to 1 m intervals at the electrode elevations for the 3D surface-to-borehole surveys (equivalent to sample elevations of the ρ_{3D} pseudo-logs). Fluid resistivity and porosity logs were not acquired for BH3.

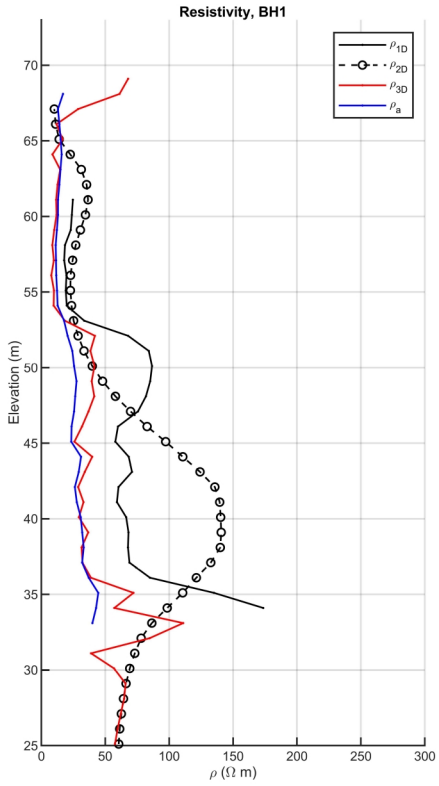
Resistivity, BH1
ρ_{1D}
ρ_{2D}
ρ_{3D}
ρ_a
Elevation (m)
ρ (Ω m)

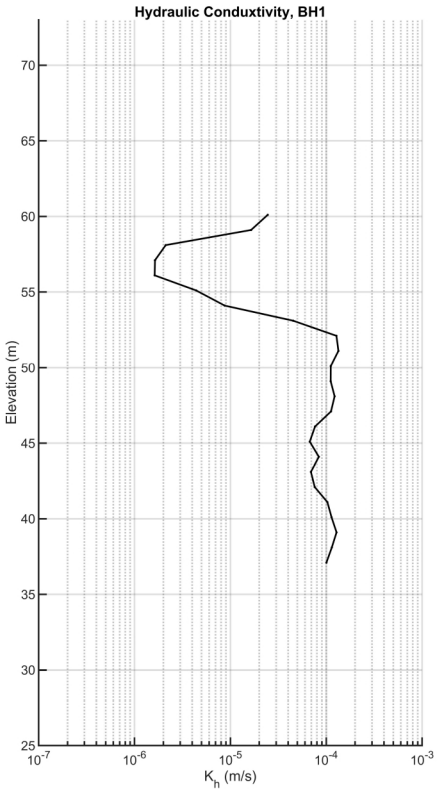
Hydraulic Conduxtivity, BH1
Elevation (m)
K_h (m/s)

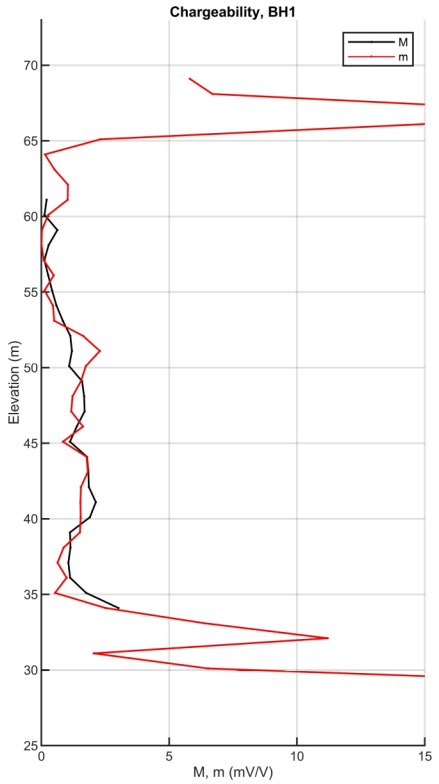
Chargeability, BH1
M
m
Elevation (m)
M, m (mV/V)

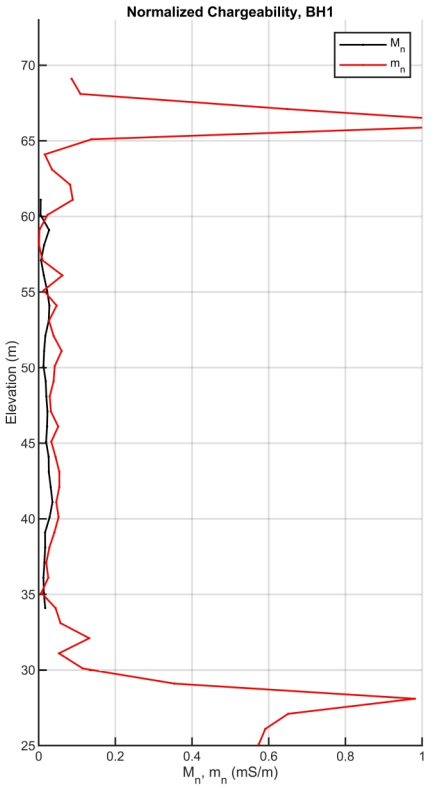
Normalized Chargeability, BH1
M_n
m_n
Elevation (m)
M_n, m_n (mS/m)

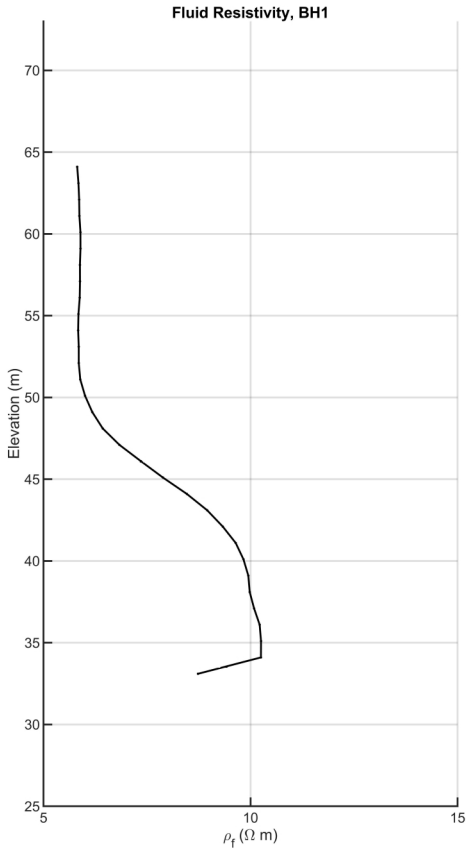
Fluid Resistivity, BH1
Elevation (m)
70
65
60
55
50
45
40
35
30
25
5
10
15
ρ_f (Ω m)

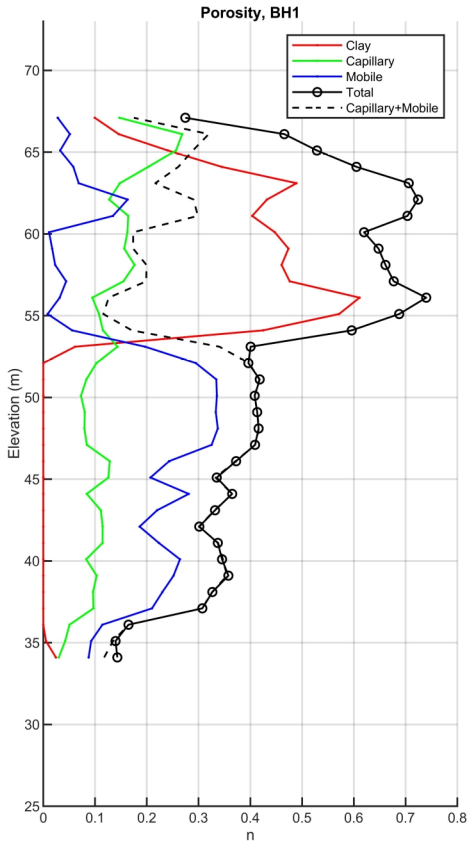
Porosity, BH1
Clay
Capillary
Mobile
Total
Capillary+Mobile
Elevation (m)
70
65
60
55
50
45
40
35
30
25
0
0.1
0.2
0.3
0.4
0.5
0.6
0.7
0.8
n

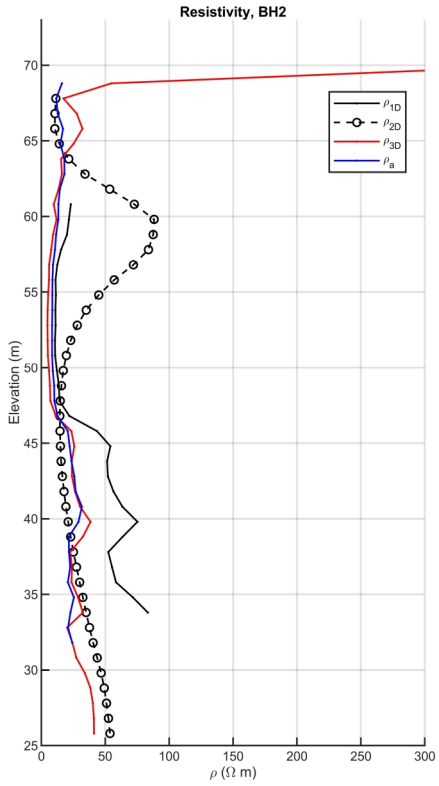
Resistivity, BH2
Elevation (m)
ρ (Ω m)
ρ1D
ρ2D
ρ3D
ρa

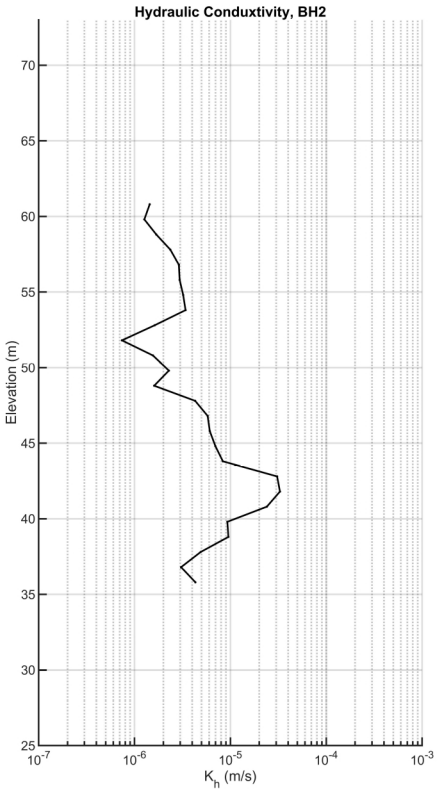
Hydraulic Conduxtivity, BH2
Elevation (m)
Kh (m/s)

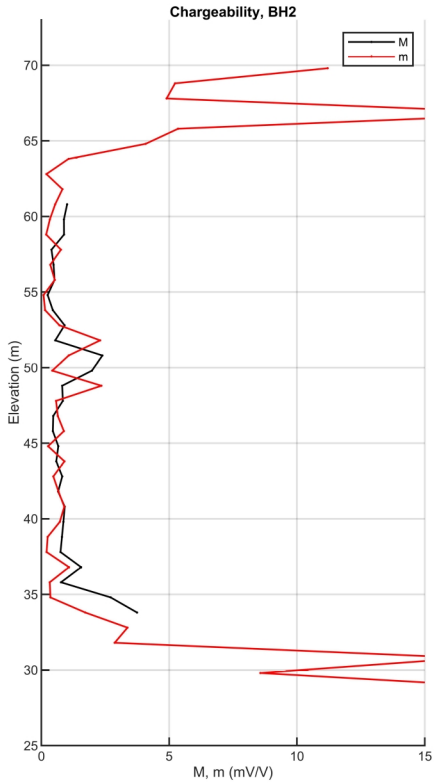
Chargeability, BH2
Elevation (m)
M, m (mV/V)
M
m

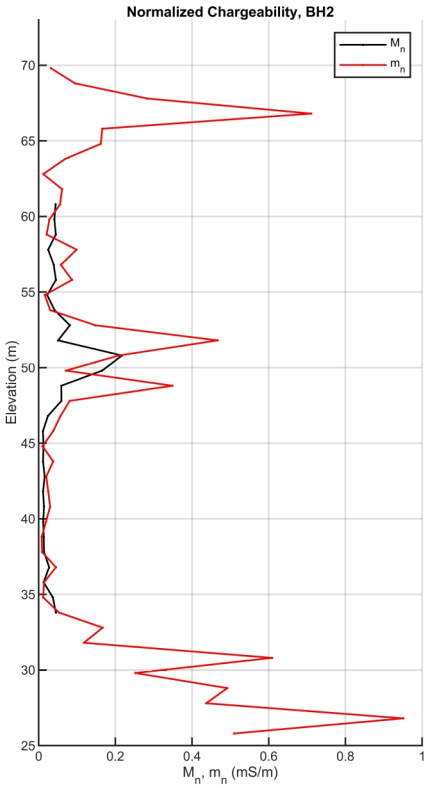
Normalized Chargeability, BH2
Elevation (m)
Mn, mn (mS/m)
Mn
mn

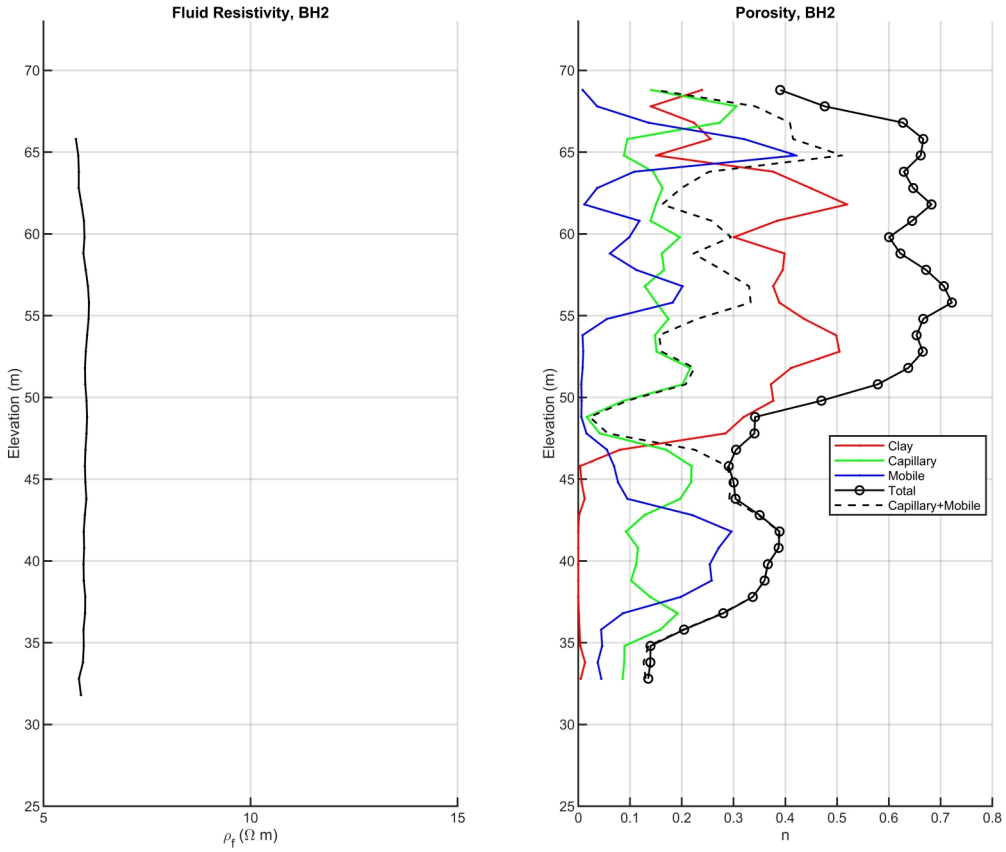
Fluid Resistivity, BH2
Elevation (m)
ρ_f (Ω m)
Porosity, BH2
Elevation (m)
n
Clay
Capillary
Mobile
Total
Capillary+Mobile

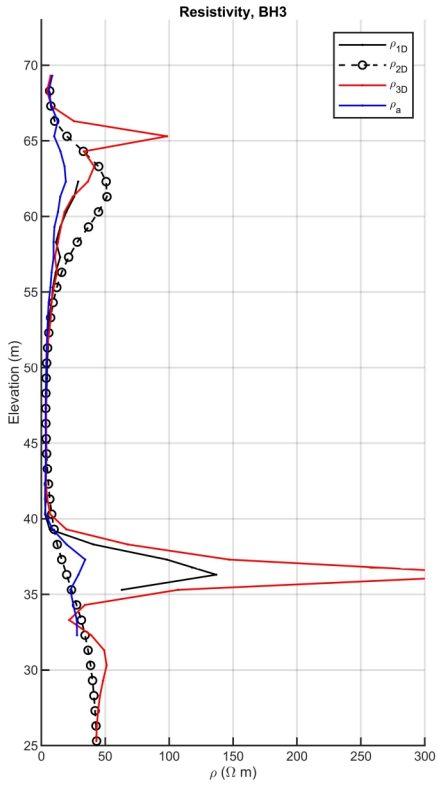
Resistivity, BH3
ρ_{1D}
ρ_{2D}
ρ_{3D}
ρ_a
Elevation (m)
ρ (Ω m)

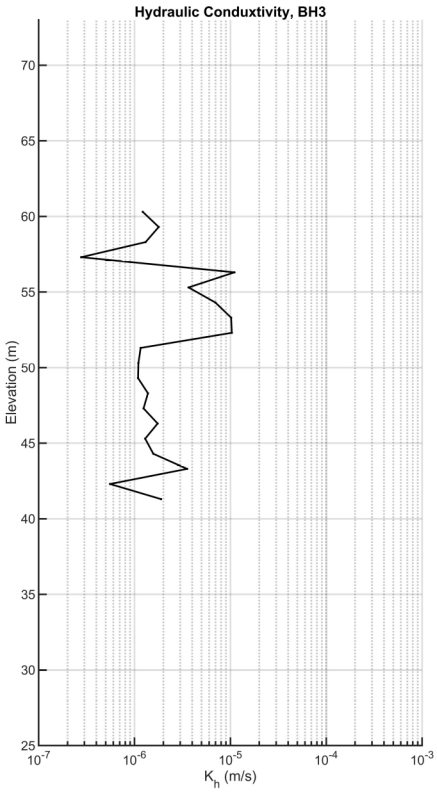
Hydraulic Conduxtivity, BH3
Elevation (m)
K_h (m/s)

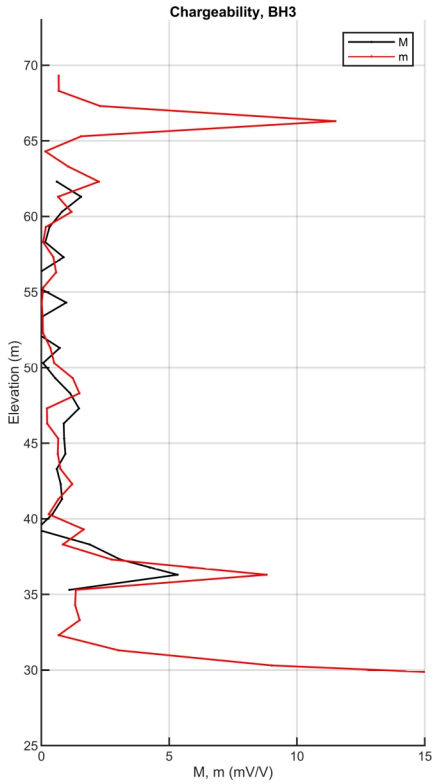
Chargeability, BH3
M
m
Elevation (m)
M, m (mV/V)

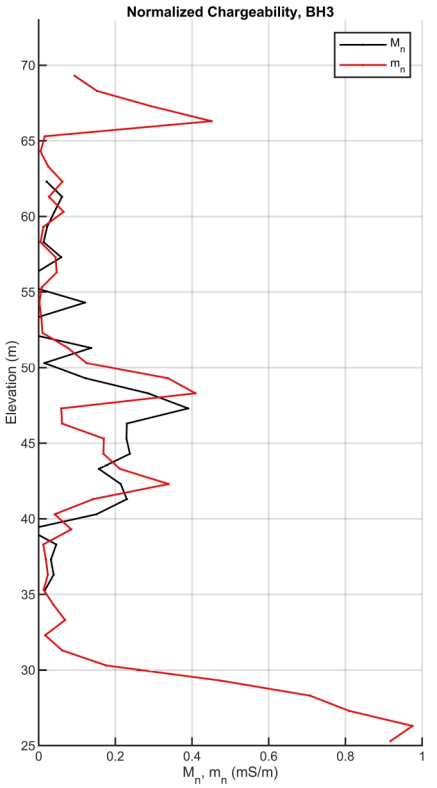
Normalized Chargeability, BH3
M_n
m_n
Elevation (m)
M_n, m_n (mS/m)

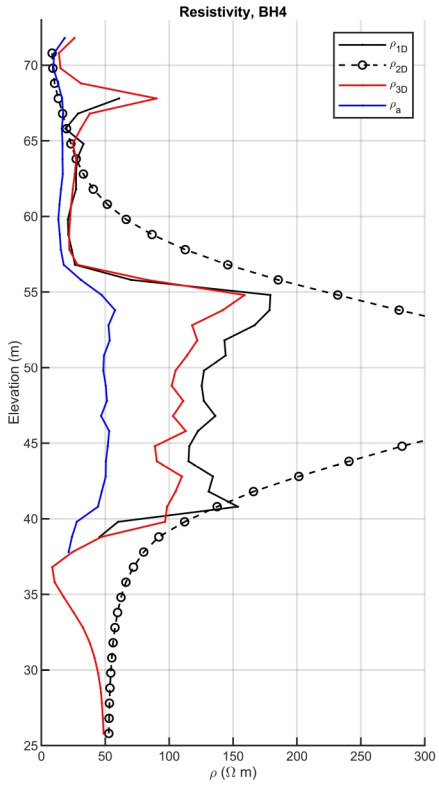
Resistivity, BH4
ρ_{1D}
ρ_{2D}
ρ_{3D}
ρ_a
Elevation (m)
ρ (Ω m)

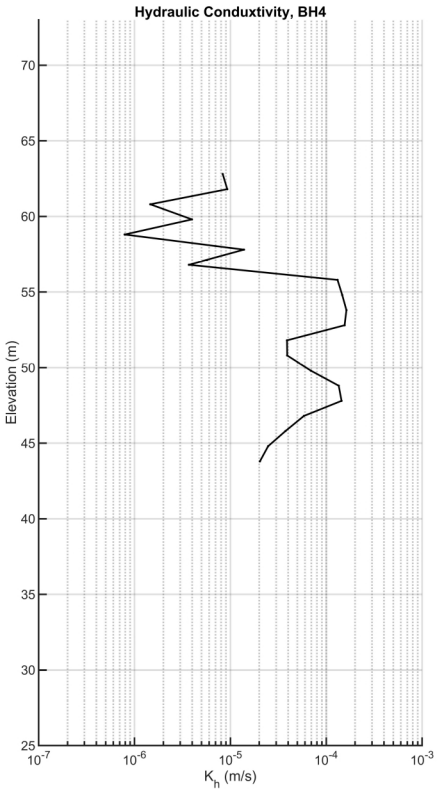
Hydraulic Conduxtivity, BH4
Elevation (m)
K_h (m/s)

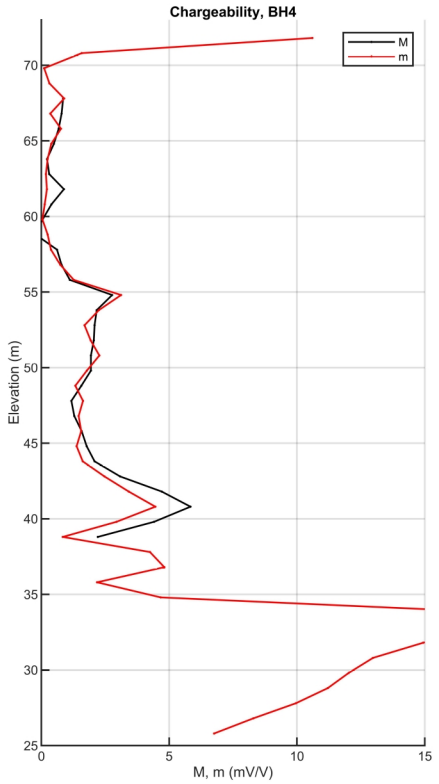
Chargeability, BH4
M
m
Elevation (m)
M, m (mV/V)

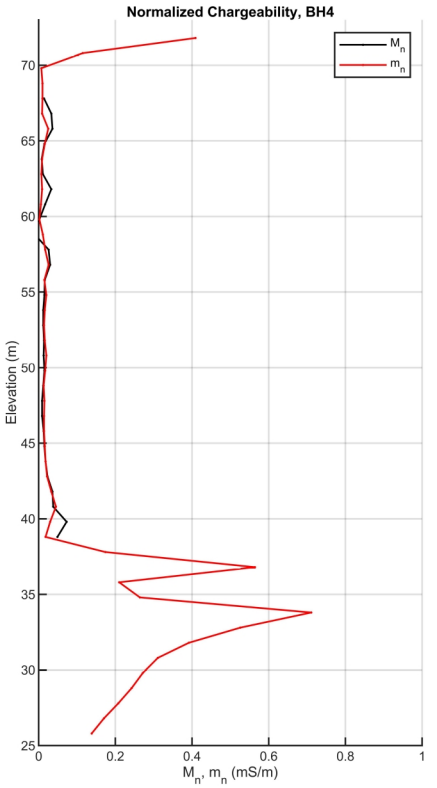
Normalized Chargeability, BH4
M_n
m_n
Elevation (m)
M_n, m_n (mS/m)

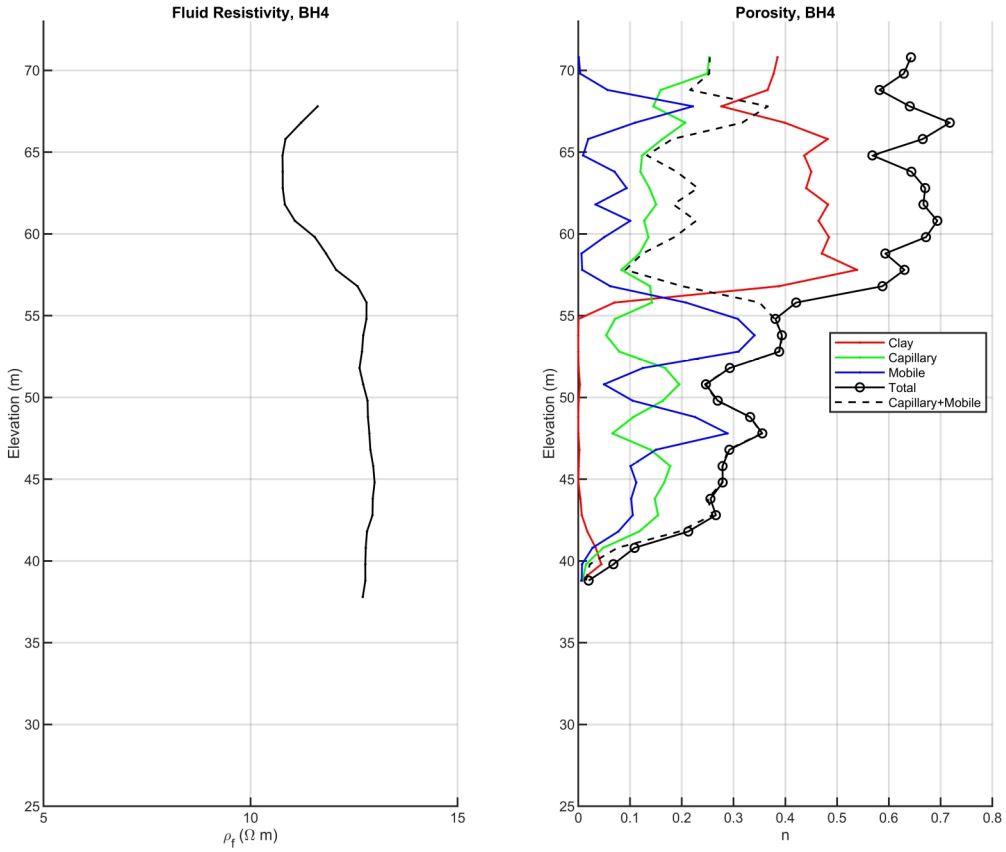
Fluid Resistivity, BH4
Elevation (m)
ρ_f (Ω m)
Porosity, BH4
n
Clay
Capillary
Mobile
Total
Capillary+Mobile